# Principles and Properties of Highly Dynamic DC Miniature Motors

Dr. Otto Stemme
Peter Wolf

Interelectric AG
CH-6072 Sachseln / Switzerland

# Preface

From the introduction of the **maxon DC motor** in 1970 it took just 2 years for the first edition release of the booklet "Small DC Motors with Ironless Armature" by Dr. Stemme.
This work found worldwide acceptance with clients and interested students alike. The old edition was expanded through the addition of sections on thermal relationships and electronic commutation of highly dynamic motors.
Peter Wolf, Director F&E of Interelectric AG, updated and revised the work of Dr. Stemme, bringing us the second edition.
With a fundamental description of technical interdependencies a better overview of the possibilities and limitations of our Maxon motors becomes possible. This second edition will be a substantial contribution to this end for both present and future interested parties.

**Enjoy the education.**

The maxon-Team
**Interelectric AG**

Translation from German by Thomas Theilmeier

For the German edition: First edition 1972
Second and completely revised edition 1994

# TABLE OF CONTENTS

# 1. Self Supported Winding DC Motors

## 1.1. Symbols and Sign Conventions

The symbols and sign conventions will generally be based on a three dimensional right-handed Cartesian coordinate system. The positive z direction is obtained by rotating the x-axis 90 degrees clockwise about the y-axis, in other words the positive z direction points out of the drawing plane. Vectors will be identified by bold letters.

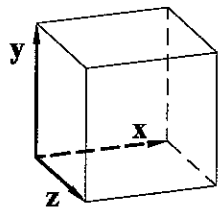


Figure 1.1.

All symbols and SI-units used (m-kg-s-A-V-K-rad) are listed alphabetically and defined in the appendix..

## 1.2. Current Carrying Conductors in a Magnetic Field

As early as the previous century the physicist Oersted found that forces act on current carrying conductors in a magnetic field. We can demonstrate this fundamental effect easily by following the elementary sketch of Figure 1.2. Attach a metal rod to two flexible conductors (wires). Allow the rod to sway freely in the magnetic field. When a current is applied we observe that the rod deflects at a right angle to the magnetic field and returns to its original position once the current is removed.

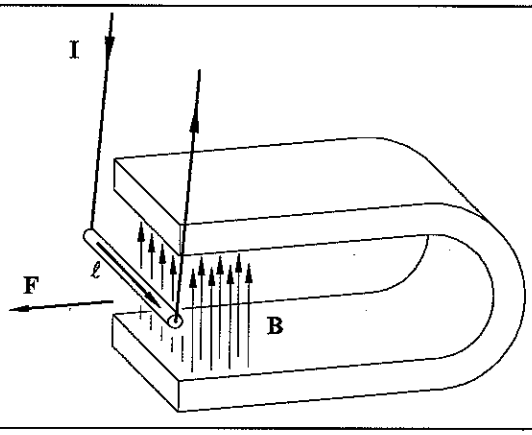


Figure 1.2.

The experiment demonstrates the following physical correlation: The deflecting force **F** is perpendicular to the plane defined by the current **I** (along the conductors length $\ell$) and field direction **B** and can be represented in vector form as a Lorentz-force:

Eq 1.1 $\mathbf{F} = [\mathbf{I} \times \mathbf{B}] \cdot \ell$ where $\mathbf{I} \times \mathbf{B}$ represents the cross product of the vectors **I** and **B**.
The following applies to the sense of the directed quantities (vectors) of Force **F**, Current **I** and Induction **B**: When looking in the direction of **F**, by rotating the current arrow **I** 90 degrees clockwise it will be pointing in the same direction as the induction **B**.

The scalar of the force is calculated by:

Eq 1.2 $F = |\mathbf{F}| = \ell B I \sin\beta$

the angle $\beta$ is formed by current **I** (with associated conductor length $\ell$) and field direction **B**.

## 1.3. Conductor Orientation to Generate Torque

### 1.3.1. Conductor Loop

To convert our simple experimental apparatus of Figure 1.2 to a torque providing motor, we must change it so the conductor can maintain constant motion in the magnetic field. We accomplish this as represented schematically in Figure 1.3, with the help of a conductor loop, attached so that it can turn freely on the rotational axis z.

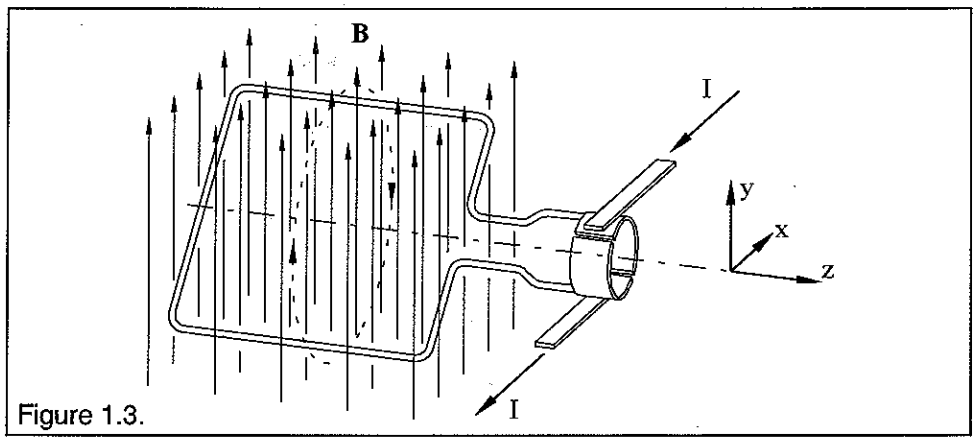

Figure 1.3.

For the orientation of the torque vector **M** the following definition applies:
$\mathbf{M} = \mathbf{r} \times \mathbf{F}$
The torque vector **M** is perpendicular to the plane defined by the position vector **r** (as a vector from the center of rotation to the point of application of the force **F**) and the force vector **F**. If we look in the direction of the torque vector **M**, then by turning the position vector **r** clockwise it will become coincident with the force vector **F**.
For example if a force vector **F** is in the xy plane with its origin at the center of rotation, the torque vector $\mathbf{M} = \mathbf{M_z}$ goes through the origin by definition and points out of the drawing plane.

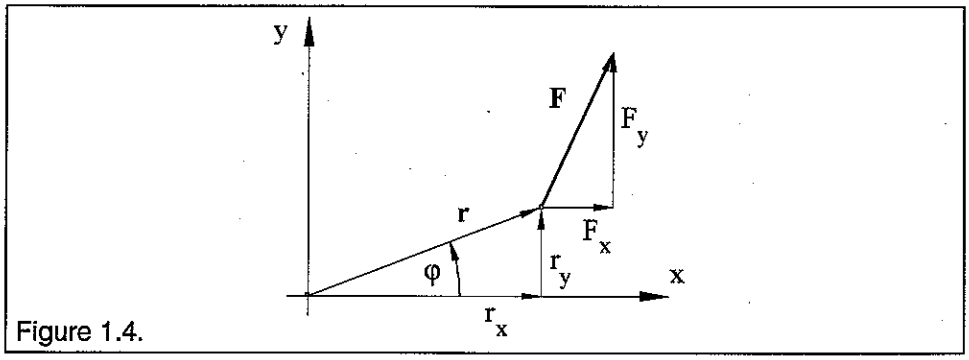

Figure 1.4.

The following equation generally defines the torque developed by the conductor loop on the z-axis with the positive direction defined as counterclockwise:

Eq 1.3 $M_z = 2(r_x F_y - r_y F_x)$

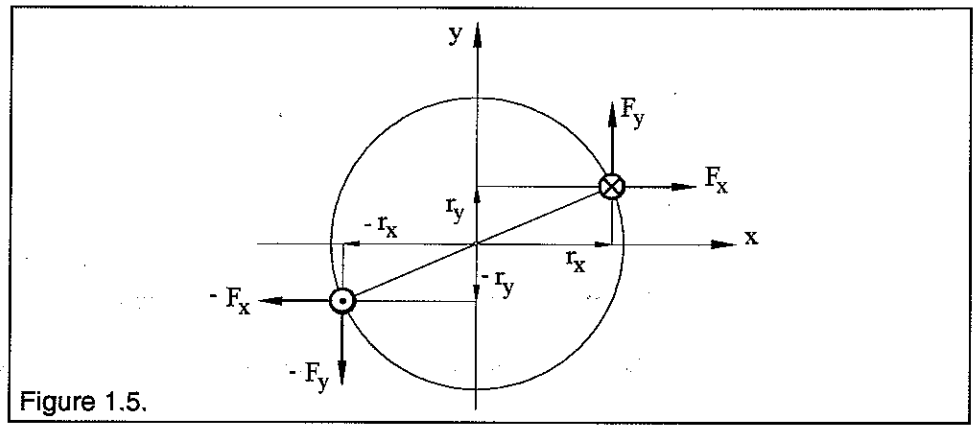

Figure 1.5.

The factor 2 appears in the equation since there are two "active" conductor segments parallel to the axis of rotation. We define r as the distance between each conductor segment and the center of rotation, therefore the radius of the loop. Its projections onto the x and y axes are $r_x$ and $r_y$ respectively. As previously shown force **F**, current **I**, and induction **B** are mutually perpendicular, therefore force **F** on the two conductor segments will have no y component but will consist entirely of an x component $F_x$ ( $F_y = 0$ ).

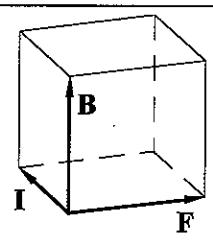

Figure 1.6.

Therefore we have

Eq. 1.4 $M_z = -2 r_y F_x$

The negative sense is due to the defined sign conventions and means only that the moment is counterclockwise about the z-axis. Substituting $r_y = r \sin\varphi$ yields

Eq. 1.5 $M_z = -2rF\sin\varphi$

According to Eq. 1.3 the portions of the conductor loop perpendicular to the rotational axis do not affect the torque about the z-axis. As is shown below this is due to the fact that the force acting on these segments has no x or y components. From the relationships Eq. 1.2 and Eq. 1.5 and dropping the negative sign and z subscript we can represent the magnitude of the torque developed by the conductor loop as:

Eq. 1.6 $M = 2r\ell BI\sin\beta\sin\varphi$

For the special case of our conductor loop, Figure 1.3, current and induction field are perpendicular to the two conductor segments and parallel to the rotational axis so that $\sin\beta = 1$, this yields:

Eq. 1.7 $M = 2r\ell BI\sin\varphi$

The effect of the torque will turn the loop about the rotational axis z assuming the orientation is proper. Normally this will occur until the loop reaches the orientation $\varphi = 0$ where, according to Eq. 1.7, the torque equals 0. Continuos rotation is not possible since for $\varphi < 0$ $\sin\varphi$, and the torque, will reverse sign. This will cause the loop to return to its position of equilibrium, that is $\varphi = 0$.
So that the loop continues to rotate past $\varphi = 0$ we must reverse the direction of current flow in the loop, this way $\sin\varphi$ and current I will reverse direction therefore maintaining the original sign (direction) of the torque.
This requirement is fulfilled if ,as in Figure 1.3, we connect the loop ends to "commutator" segments and connect the current supply with two sliding contacts (brushes). The brushes are oriented with respect to the loop so that the current is reversed at $\varphi = 0$.
The loop would still stall at this position , even though the current will now be reversed, since the torque = 0 at $\varphi = 0$. Furthermore the brushes would be momentarily shorted across the commutator segments so that no current would flow in the conductor loop. In order to develop torque in every rotor position a minimum of three active conductor and commutator segments must be used.

### 1.3.2. Rectangular and Angled Windings

From Eq. 1.7 we derive that to achieve maximum torque we must increase the induction B as much as practicable. Therefore we will modify the original setup further to minimize the air gap in our magnetic path.
In our model we fill the space in the conductor loop with a cylindrical iron core and utilize cylindrically shaped pole shoes as shown in Figure 1.7.

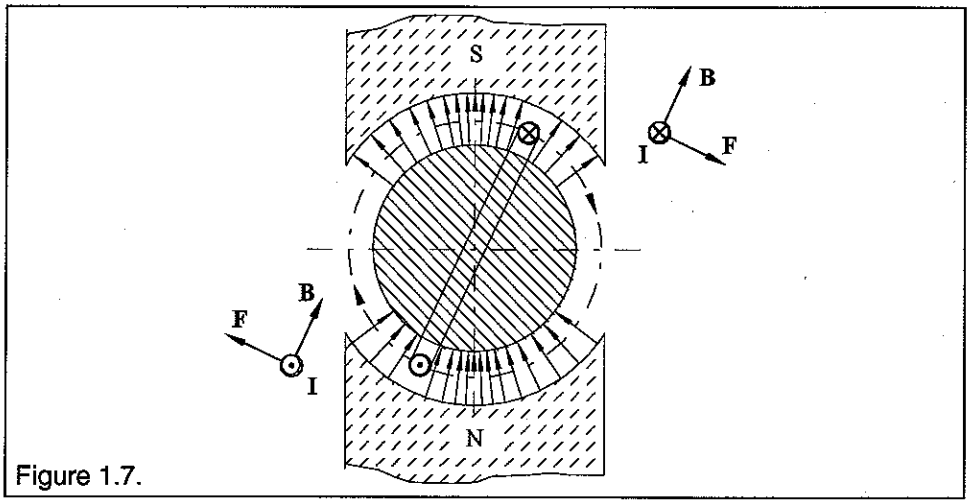

Figure 1.7.

In principle we could wrap our loop, or a greater number of loops (which are required for a motor, as we shall see later) around an iron core. In this manner the iron core and winding will rotate as one unit in the magnetic field. However, we will not explore this approach mainly because the mass of the "stator" or "rotor" will yield a relatively high moment of inertia which will cause slow acceleration and iron core losses. Our conductor system will be free to move in the air gap between core and pole shoes.

The difficulties in manufacturing and assembling a cage type winding, specifically in filling the inner space, are obvious. Therefore we will abandon our original loop form and construct our conductor system in such a fashion that the resulting rotor coil tube will be open at one of its ends. The desired form of rotor coil will be achieved if the coil is constructed of conductor loops formed as in Figure 1.8.

Here, as with our simple conductor loop, only the conductor segments parallel to the axis of rotation contribute to the torque. Therefore the previous discussion, relationships and conclusions apply to this loop as well.
Regrettably, this coil style has a decisive flaw. If we continue to wind loops so that we form a tubular coil, the overlapping curved conductor segments will form a relatively thick ring. In order to assemble the motor we would be forced to either increase the air gap between pole shoes and core or allow the thick ring to protrude out of the magnet path. If we enlarge the air gap the induction would be reduced or the protruding "passive" portion of the coil would only serve to increase the resistive losses. We must find a better way to construct the rotor.

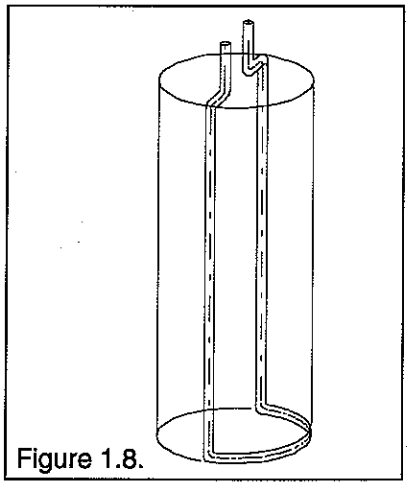
Figure 1.8.

Conductors wound as slanted loops ,as in Figure 1.9, will construct a usable tubular coil.
We found in section 1.2.1 that for a torque on the rotational axes only those forces acting in the y direction contribute, or in general only tangential components of forces need to be considered in determining the torque. Since current **I**, Induction **B** and force **F** are mutually perpendicular only the current I directed parallel to the axis of rotation will contribute to tangential forces. Therefore for purposes of calculation, we can replace the slanted conductor with one oriented parallel to the rotational axis.

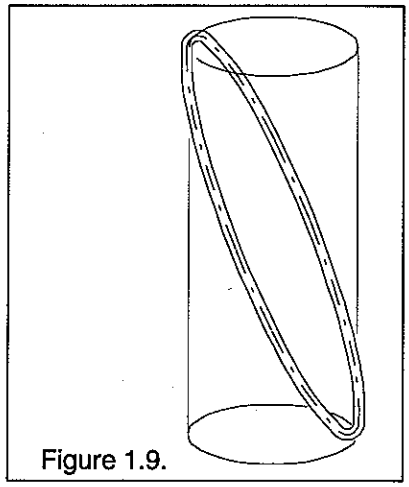
Figure 1.9.

Naturally it is not possible to simply wind a coil so that the space between adjacent conductors is eliminated. This is also true for coils constructed as in Figure 1.10

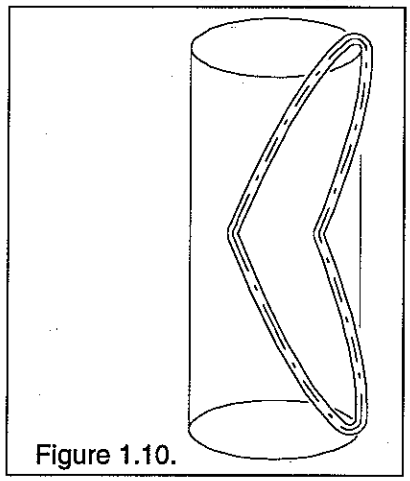
Figure 1.10.

### 1.3.3. Rhombic-winding

In order to maximize winding density, rotor coils for Maxon motors are fitted with a rhombic winding. We should recognize Figure 1.10 as the loop shape of a "Rhombic-winding". The rotor coil does not start out as a cylinder. It is first wound as a flat strap. By using an appropriate forming fixture the strap is stretched to look like Figure 1.11. This way the conductors on each side of the strap are pulled together until they are brought into intimate contact.

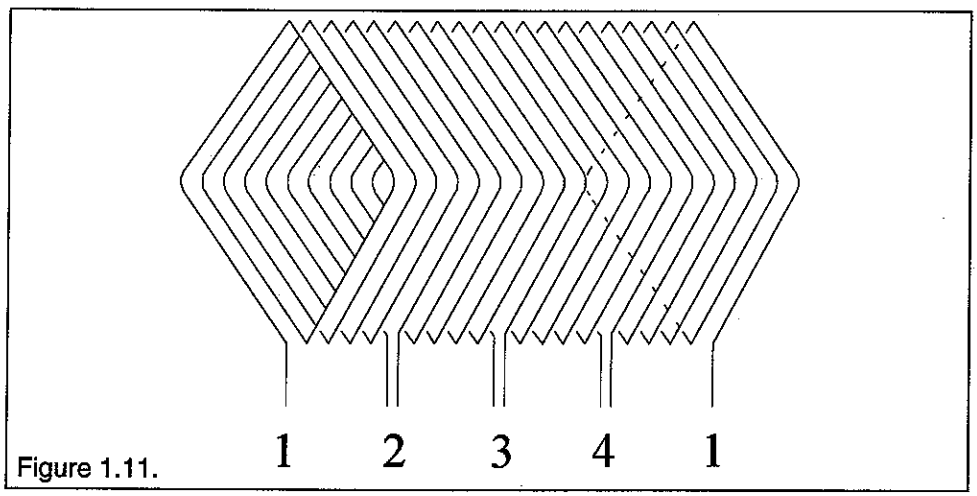

Figure 1.11.

The strap is then rolled into a cylinder and glued. The winding taps 1,2,3 and 4 are connected to the associated commutator segment.
If we apply the resolution of forces from the simple angled winding to the Rhombic-winding, and employ a similar thought process, we find that we can imagine each half of the winding as a straight conductor running parallel to the axis of rotation.

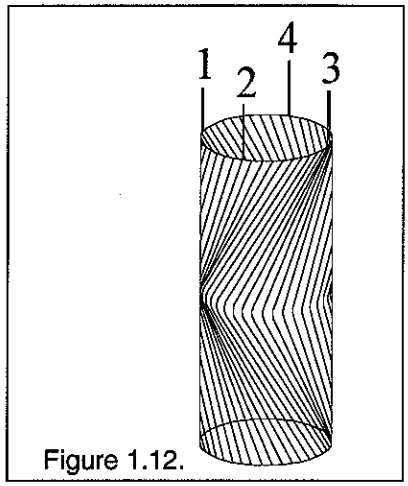

Figure 1.12.

## 1.4. Magnet System

### 1.4.1. Basic Construction

With historically short development cycles and rising costs fewer and fewer magnet systems are laid out experimentally. By empirical methods the design (ie materials and size) is changed in small increments, based upon measurements until the requirements are met. Today the design of magnetic circuits is primarily performed on computers, where, depending on the type of problem, experience and other means available, the most expedient method of solution is chosen. In principle there are three different solution methods: The conventional method whereby the magnetic circuit is replaced by an analogous electrical circuit, the analytical mathematic method which will, in simple cases, result in an equation relating geometric and magnetic values, and finally numerical methods which permit an actual optimization.

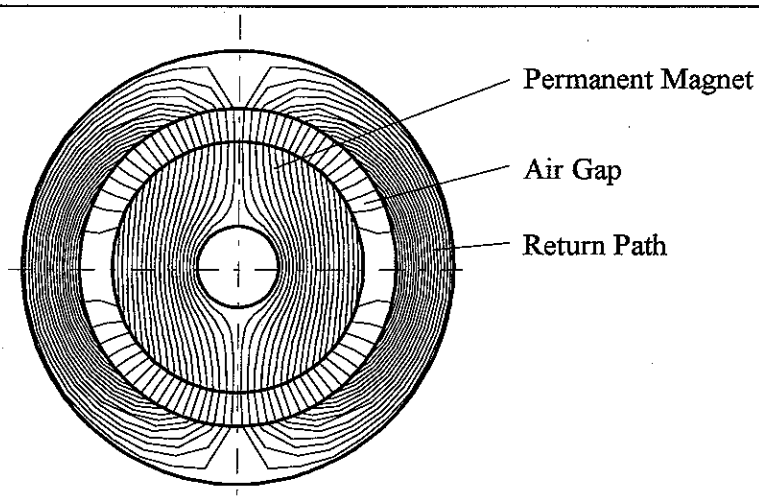

Figure 1.13.

Usually the basic construction of a Maxon motor magnet system is represented by a cylindrical Alnico inner magnet. The Figure clearly shows the flow of the magnetic flux in the magnet, air gap and return path. In order to have a compact form factor the iron core of Figure 1.7 is replaced with a cylindrical permanent magnet. The surrounding iron return path doubles as the motor housing. For this design type the material for the magnet core is Alnico, a hard magnetic alloy, which permits high induction values in the air gap at low cost.
This anisotropic magnet material has another important property: Through proper handling during manufacturing of the magnet cylinder it is possible to

create a preferential axes of magnetization. This axes cannot be altered without exposure to extremely dense magnetic fields. Thereby the permanent magnets of Maxon motors have an ingrained preferred axes of magnetization, and the magnetization direction is locked in. After assembly of the motor the magnets are magnetized in the preferred direction by exposure to a dense magnetic field.

### 1.4.2. Physical Characteristics

When applying the conventional method for the design of magnetic circuits one starts with the known relationship between magnetic flux and magnetic potential. The law of magnetic flux gives us the relationship between magnetic field strength and excitation current, the magnetic flux is the result of the integration of the flux lines over the pertinent surface.

Eq. 1.8 $$\int_{\ell} \mathbf{H} \cdot d\ell = wI \qquad \Phi = \int_{A} \mathbf{B} \cdot d\mathbf{A} \qquad \oint \mathbf{B} \cdot d\mathbf{A} = 0$$

The permanent magnet is described by its demagnetizing curve, the soft magnetic return path material's ultimate permeability can be taken into consideration by using a magnetic potential decay factor $\tau$ (approximate value $\tau \approx 0.85$).
The leakage current's, in the electrical circuit, corresponding leakage flux is covered by a not precisely calculable magnetic leakage factor $\sigma$ ($\sigma < 1$).

Substituting and simplifying yields, for the zero current condition,

$$H_L \ell_L + \tau H_M \ell_M = 0$$

Eq. 1.9 $$H_M = -H_L \frac{\ell_L}{\ell_M} \frac{1}{\tau}$$

The field strength $H_M$ in the permanent magnet has the opposite direction of the field strength $H_L$ in the air gap, therefore also in the opposite direction of induction $B_M$ there fore the effect of the air gap is to demagnetize.
For the simple case of a magnetic rod the basic shape of the field strength **H** and induction **B** can be visualized as below.

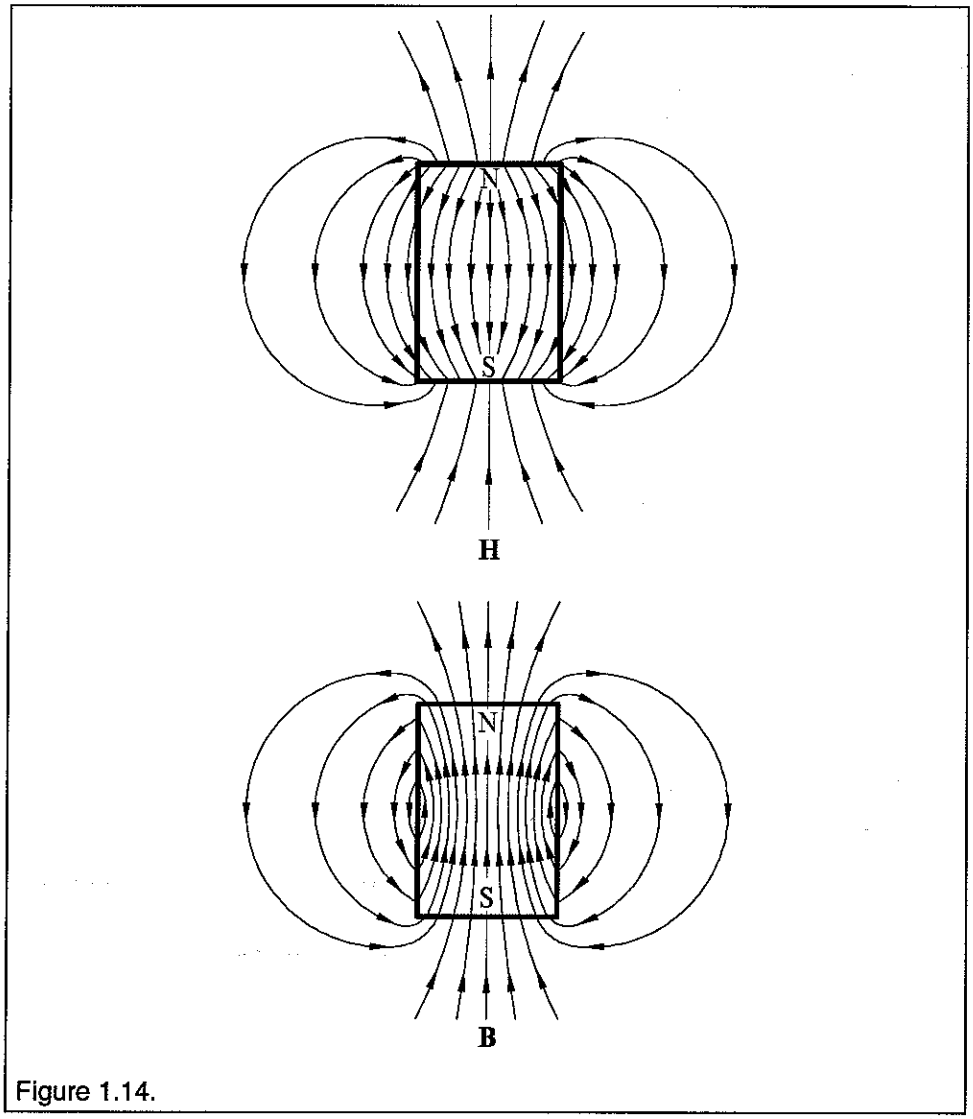


Figure 1.14.

Externally, of the magnet, the shape of the H and B fields are identical whereas internally the shape of the two fields is different and the direction is reversed. The following proportion is valid for the air gap

Eq. 1.10 $B_L = \mu_o H_L$

with this we get the flux relationship

Eq. 1.11 $\sigma B_M A_M = B_L A_L = \mu_o H_L A_L$

From Eq. 1.9 and Eq. 1.11 we can derive the equation for shearing lines, whose slope ,ignoring $\tau$, depend only on construction and dimensions of the magnetic circuit but are independent of permanent magnet material.

Eq. 1.12 $$H_M = -\frac{1}{\mu_o}\frac{\ell_L}{\ell_M}\frac{A_M}{A_L}\frac{\sigma}{\tau}B_M$$

The magnetic operating point of the permanent magnet is defined by the intersection of the shearing lines and the demagnetization curve. Taken strictly the permanent magnet is not operating at an operating point but in an operating

range. If we compare the path along various flux lines then the variation of $\ell_M$ becomes apparent.
The permanent magnet therefore does not operate at the residual magnetism level $B_r$, but at the lower value of $B_A$ and $H_A$.

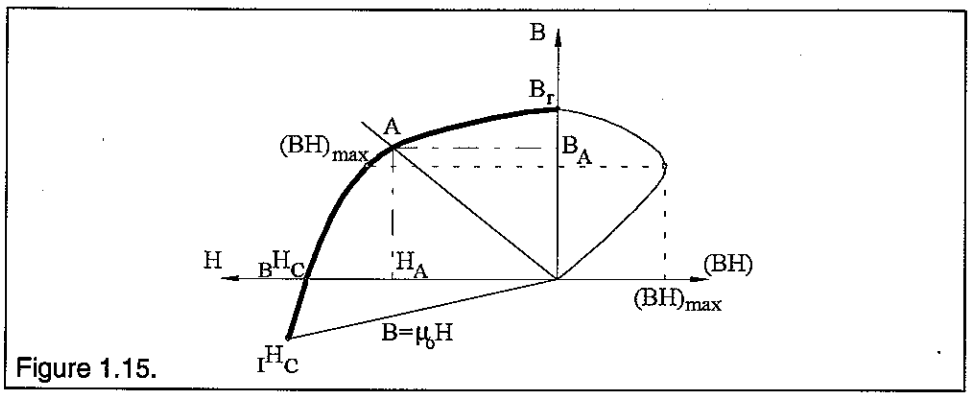

Figure 1.15.

We can calculate the optimum operating point by defining the energy for the air gap and magnet.
The magnetic energy in the air gap can be represented by

Eq. 1.13 $$W_L = V_L \int_0^H \mathbf{B}_L d\mathbf{H}_L = V_L \int_0^H \mu_o \mathbf{H}_L d\mathbf{H}_L = \frac{1}{2}\mu_o H_L^2 V_L$$

specifically the homogeneous ratio of the energy stored in the permanent magnet is solved for by

Eq. 1.14 $$W_M = V_M \int_0^B \mathbf{H}_M \, d\mathbf{B}_M = \frac{1}{2} H_M B_M V_M$$

Multiplying Eq. 1.9 with Eq. 1.11, results in the relationship

Eq. 1.15 $$\sigma\tau \left|B_M H_M\right| V_M = \mu_o H_L^2 V_L = \frac{1}{\mu_o} B_L^2 V_L$$

Therefore the magnetic energy stored in the air gap is proportional to the magnet volume and the product $|B_M H_M|$ at the operating point of the magnet. If we define the operating point of the magnet as $B_A$ and $H_A$, then we get Eq. 1.16 for the magnet volume

Eq. 1.16 $$V_M = \frac{1}{\mu_o \sigma\tau} \frac{B_L^2 V_L}{\left|B_A H_A\right|}$$

The larger $|B_A H_A|$ is, the smaller the requirement for permanent magnet volume becomes for any desired air gap energy level.
The product $|B_A H_A|$ equals zero at $B_r$ and $_BH_C$ and goes through a maximum, as shown in Figure 1.15, along the demagnetization curve.
The $(BH)_{max}$ value, the maximum energy product, is another important parameter in characterizing permanent magnet materials.

For optimum utilization of the magnetic material shearing line Eq. 1.12 in the magnetic circuit should be selected so that the operating point is coincident with $(BH)_{max}$.

Deviation of the operating point from $(BH)_{max}$ is indicated when high air gap induction, more stabile characteristics of the magnetic circuit (demagnetization, temperature) in the flat section of the demagnetization curve or reduced return path size is more desirable than minimum magnetic material volume. Special consideration must be given to this for RE magnets with their very high energy products $(BH)_{max}$ and extremely high coercive forces.

For the magnetic circuit above a simpler proportion can be used for the return path cross section $A_{Ra}$. The flux $\Phi_L$ saturating the air gap must be captured by the return path and yields the following relationship, neglecting stray flux:

Eq. 1.17 $$\Phi_L = \int_A \mathbf{B}_L d\mathbf{A}_L = \int \mathbf{B}_{Ra} d\mathbf{A}_{Ra}$$

and the average air gap induction is

Eq. 1.18 $$A_{Ra} = \frac{B_L}{B_{Ra}} A_L$$

Saturation induction must be considered when selecting return path material.

## 1.5. Commutator System

Basically **maxon**-Motors are constructed without through shafts, however as size increases they are fitted with a through shaft. Models with one protruding shaft end have advantages by design for constructing commutators fitted with metal brushes. Since the torque output shaft need only come out the front of the stator, it is possible to fit a commutator with an extremely small outer diameter to the opposite side.

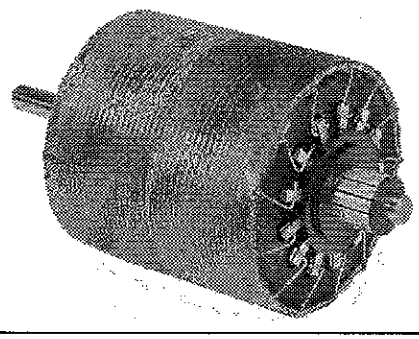

Figure 1.16.

For any given rotational speed $n_b$ this results in lower surface speeds $v_k$ of the commutator and shorter wiped distances for the brushes over the life of a motor. Furthermore the frictional losses between brush and commutator $M_{Vk}$ can be kept small.
Figure 1.16 shows the rotor coil, welded connections between winding taps and appropriate commutator segment and the cylindrical commutator. The properly profiled commutator segments are made of a silver alloy and the precious metal alloy brushes (not shown) are preloaded, flexible and multi segmented for positive contact. The precious metal alloy may be changed depending upon application.

Since the life of a motor is generally limited either by the bearings or brush-commutator system the wear on the later must be kept to an absolute minimum. Besides mechanical rubbing, the wear (of the brush or commutator) is due to ark erosion. Therefore the most effective ark suppression is required to reduce the arcing between brush and commutator.
We can differentiate two ark forming zones where the undesired material migration occurs. Massive arcing can occur between brush and segment during the normal conducting phase as shown in Figure 1.17, a much stronger "arc at break" occurs the moment contact between brush and passing segment is broken.

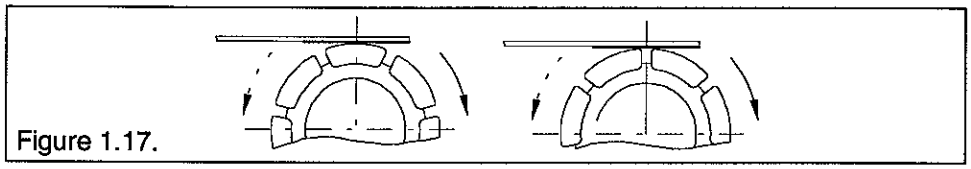

Figure 1.17.

The current I carried through the brushes to the commutator segment splits as I/2 and flows through each half of the parallel connected winding segment. The brushes short each partial winding segment in turn. The direction of current flow in the winding segment is reversed during commutation, which can only be accomplished through a superimposed current circuit within the winding segment. The rotational speed dependant time for current reversal determines the current variation speed and together with winding segment inductance determines the self induced voltage $u_L$ in the short circuit

Eq. 1.19 $$u_L = L_T \frac{dI}{dt}$$

An "arc at break" occurs when the winding segment is short circuited before the internal current fades away and the remaining voltage is sufficient for a micro arc. Both high rotational speeds and loads contribute to this effect since in both cases locally high current variation speeds occur.

The voltage $u_L$ ,due to current variation, alone is not responsible for the equalizing current, a further contribution is due to the motion of the winding segment in the magnetic field. The voltage induced in the winding segment by the changing flux is

Eq. 1.20 $$u_i = w_T \frac{d\Phi}{dt}$$

In order to have these voltages approach zero it is required that the brushes be aligned , with respect to the magnetic field, so the short circuited winding segment is not subject to any change in flux. This is clearly the case for a motor operating at no load when the winding segment is at 90° to the preferred magnetic direction.
Assuming this alignment (commutation timing), and loading the motor so a substantial current flows through the winding then a magnetic field H is generated in the interior of the winding spool. The orientation of this field will be approximately perpendicular to the magnetic direction of the permanent magnet and will slightly alter the orientation of the magnetic field with respect to the preferred magnetization direction.

As we can extract from related literature when a magnetic field H is oriented perpendicularly to the preferred direction of magnetization then the torsion angle $\psi$ of the magnetization direction is

Eq. 1.21 $$\sin \psi = \frac{H}{H_K}$$

The anisotropic field strength $H_K$ is a material constant which characterizes the "strength" of the preferred direction. The value for Alnico is approximately 200 kA/m and is substantially higher for RE-Magnets.
A current carrying rotor can easily achieve a magnetic field H of several kA/m , resulting in a torsion angle of approximately 1° to 2°.

If the motor is operated at a more or less constant load (speed and torque) and in one direction only then stator field H and self induced voltage $u_L$ will remain unchanged in magnitude and direction. The commutation timing can be altered by $\psi' > \psi$ to better fulfil the commutation requirements. A voltage $u_i$ is purposely induced in the approaching winding segment which will, at least partially, counteract the negative effects of H and $u_L$.

If, in application of the motor, the load or rotational direction vary then the best compromise commutation timing is the neutral, that is, no load setting.
To minimize the stored magnetic energy $W_{LT}$ in the short circuited winding segment and thereby the intensity of the arc at break the winding segment turn count is reduced by dividing the winding into as small as practicable segments that is a large number of commutator segments k.

Eq. 1.22 $$W_{LT} = \frac{1}{2} I^2 L_T \qquad L_T \approx w_T^2$$

In the case of difficult operating conditions (motor reversing, on-off cycling, high environmental temperature, load conditions close to the limit) the utilization of carbon brushes instead of precious metal brushes is sensible purely for motor life considerations. The sometimes negative influence of nonlinearities, for example the current density dependant brush voltage drop, become noticeable especially for low resistance windings. The fundamental considerations discussed thus far are valid for those cases as well.

# 1.6. Design Principles

## 1.6.1. Alnico-Motor with Precious Metal Brushes

Figure 1.18 shows a sectional layout of a **maxon**-Motor without through shaft, metal brushes and Alnico-Magnet. Shown is how the Alnico-Magnet (1), is connected to the rust resistant steel return path (3) ,which doubles as motor housing, with engineering plastic (2).

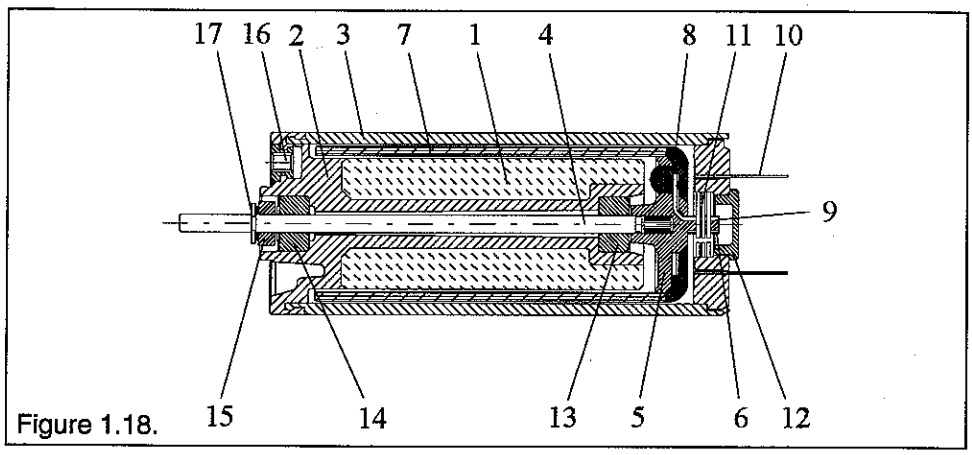

Figure 1.18.

The shaft (4) is attached to a collector plate (5) with the commutator (6). The collector plate (5) is attached to the winding tube (7) made from the Rhombic winding. The junctions (8) connect the winding taps to the commutator segments (9).
The current supply is provided through the connection tabs (10), which are welded to the metal brushes (11). The end cap (12) serves to protect the commutator system from dust and mechanical damage.
The sintered brass bearings (13 & 14) support the shaft (4). Retaining ring (15) serves the dual function of axially locating the shaft and preventing any bonding agents used to attach drive components from migrating into the bearing (14).Threaded inserts (16) anchored in the plastic (2) facilitate mounting the motor by the front face.

## 1.6.2. RE-Motor with Graphite Brushes

As an alternative a sectional layout of a **maxon**-RE-Motor with through shaft, carbon brushes and ball bearings.

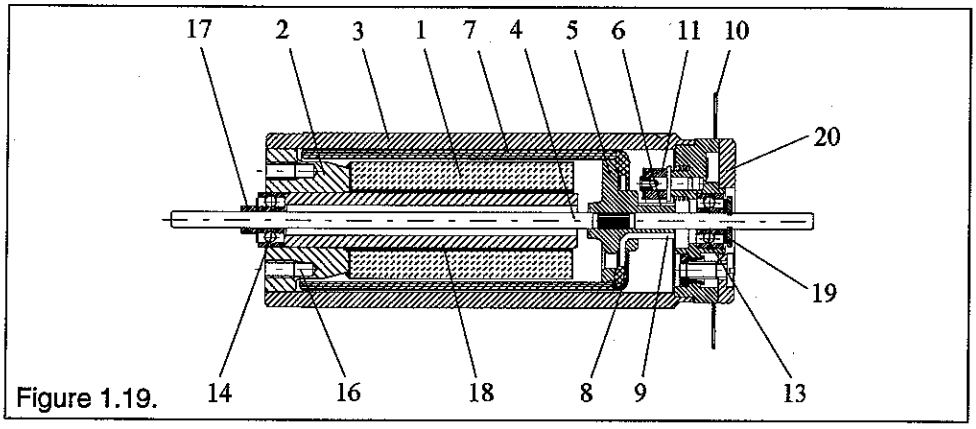

Figure 1.19.

In this design concept the RE-Magnet (1) is connected to the rust resistant steel outer return path (3) with a steel inner return path (18) and a magnet carrier plate (2). The shaft (4) supports the collector plate (5) with commutator (6). The winding tube (7) formed by the Rhombic winding is mounted to the collector plate (5). The junctions (8) connect the winding taps with the commutator segments (9).
The current supply is provided through the connection tabs (10), which are connected to the carbon brushes (11) with very flexible copper wire straps. The ball bearings (13 & 14) support the shaft. The shaft is retained axially with 2 retaining rings (17 & 19). The threads in the magnet carrier plate (2) facilitate mounting the motor by the front face.

The through shaft (4) facilitates mounting an encoder after removing cover (20).

## 1.7. Motor Characteristic Quantities

### 1.7.1. Torque

To facilitate calculating the torque of a **maxon**-Motor we must first derive ,with help from Figure 1.20, which parts of the rotor winding contribute to the generation of torque.
For clarity purposes we imagine the Rhombic winding split in half then flattened so that we have two winding segments.

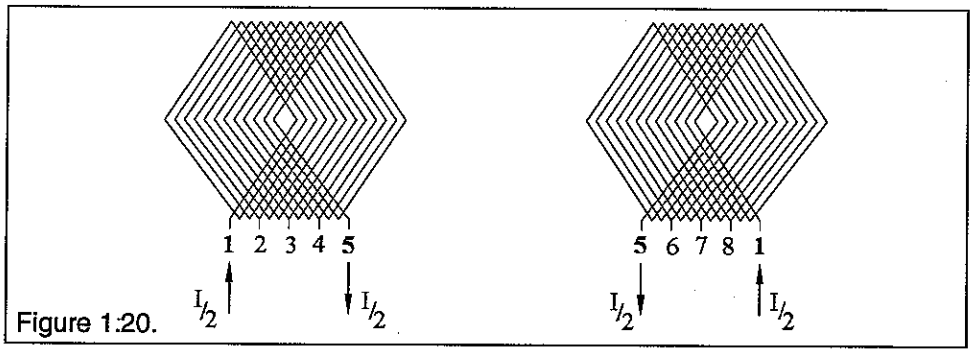

Figure 1.20.

We connect the current source so the motor current I flows from winding tap 1 to 5. We then study the distribution of current flows that are parallel to the axis of rotation, contributing to the torque.

As we can see in Figure 1.21 the current flows upwards in the vertical hatched regions and downwards in the horizontally hatched regions. This is represented by the respective current arrows.

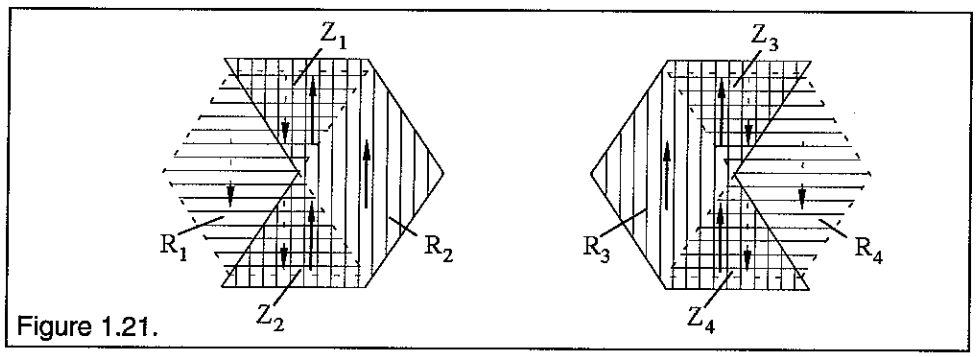

Figure 1.21.

In the triangular surfaces $Z_1$ - $Z_4$ the forces due to the current flow cancel as the overlapping winding layers cause the current to flow in opposite directions. The current flowing in rhombs $R_1$ - $R_4$ on the other hand remain effective. To return to the actual rotor winding we first move the two segments so rhombs $R_2$ and $R_3$ are coincident. We see immediately that the forces due to the current flow are additive (see Figure 1.22). If we now form the winding tube by rolling the strap to bring rhombs $R_1$ and $R_4$ coincident, again the forces due to current flow are additive.

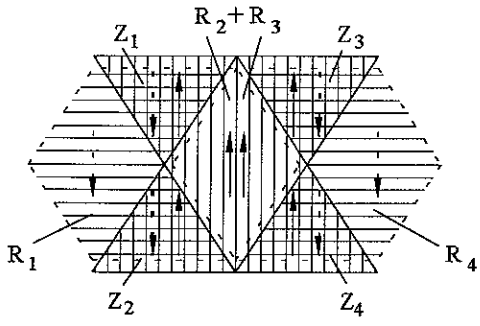

Figure 1.22.

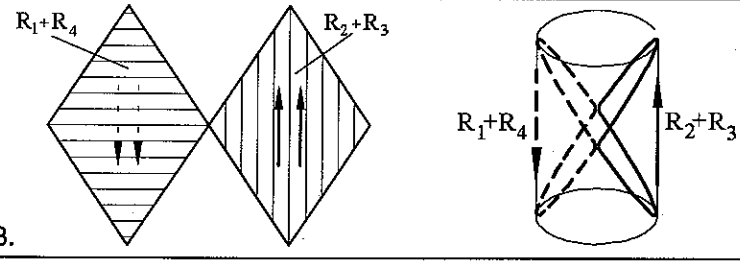

Figure 1.23.

To calculate the torque we will first idealize the commutator by dividing into extremely fine segments. For this case the diagrams of Figures 1.20- 1.23 will remain valid even if there are an uneven number of commutator segments. Furthermore we see that the when wire rhombs are separated by an extremely fine commutation they are continuously switched cyclicly so that the effective rhombic regions are "stationary".

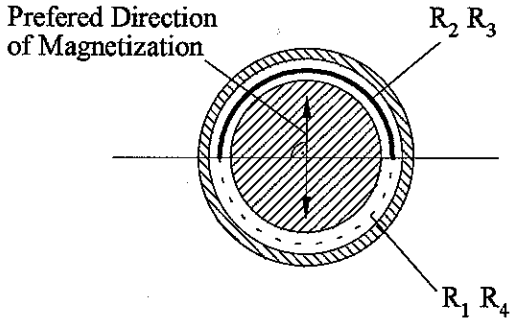

Figure 1.24.

Next we calculate the effective force of a "current rhomb" area as shown in Figure 1.24. With the help of Figure 1.23 we can visualize that each winding segment of the rotor in a current rhomb is made up of one conductor. However there are two winding layers on top of each other and, as we saw above, the effect of each is additive. If we represent the winding density (winding number) of the rotor circumference as $\nu = w/2r\pi$, then each "current filament" in the

width ds has in total 2νds conductors (each winding has a to and a from conducting segment which are both active contributors to torque).

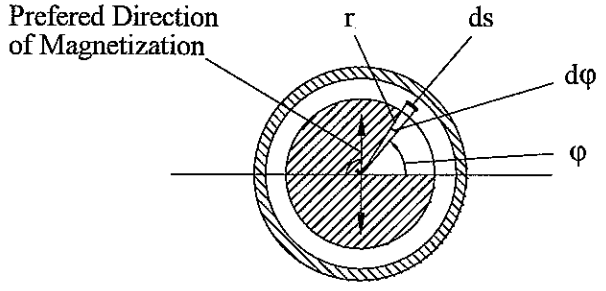


Figure 1.25.

Since both winding halves of Figure 1.20 are connected to the brushes in paralell each half will carry current equal to I/2 so that the "current filament" collectively carries the current νdsI. Due to Eq. 1.2 and with sin β = 1 we get, for the force acting on the "current filament",

Eq. 1.23 $dF = I B y \nu ds$

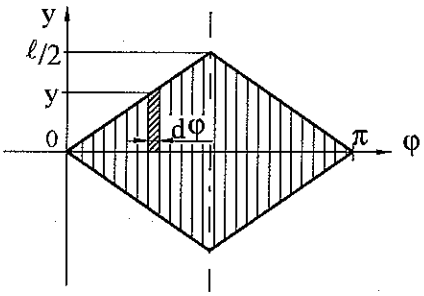


Figure 1.26.

As we can infer from Figure 1.25 ds = rdφ therefore

Eq. 1.24 $dF = I B y \nu r d\varphi$

As measurements confirm, the angular dependance of induction is accurately approximated by $B = B_o \sin\varphi$.

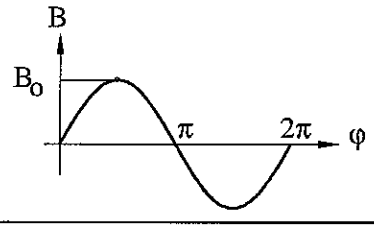


Figure 1.27.

To simplify further we will assume B as a constant in the axial direction. Now considering the linear growth of the length y of the "current filament" with φ through y=aφ, whereby φ varies in the range $0 \le \varphi \le \pi/2$ and a =ℓ/π= constant, we get

Eq. 1.25 $dF = I B_o \nu r a \varphi \sin\varphi d\varphi$

and through integration over all "current filaments" with a =ℓ/π the total force acting on the first quarter of the rhomb of Figure 1.25

Eq. 1.26 $$F = I B_o \nu r a \int_0^{\frac{\pi}{2}} \varphi \sin\varphi \, d\varphi = I B_o \nu r a \left[\sin\varphi - \varphi\cos\varphi\right]_0^{\frac{\pi}{2}} = \frac{1}{\pi} I B_o \nu r \ell$$

The force

Eq. 1.27 $$F_{ges} = \frac{8}{\pi} I B_o \nu r \ell$$

acts tangential on the entire rotor and generates the torque

Eq. 1.28 $$M = F_{ges} r = \frac{8}{\pi} I B_o \nu r^2 \ell$$

specifically expressed with winding density w = 2πrv,

Eq. 1.29 $$M = \frac{4}{\pi^2} I B_o r \ell w$$

Rewriting Eq. 1.29 with current as the independent variable and graphing the results

Eq. 1.30 $$I = \frac{\pi^2}{4} \frac{1}{B_o r \ell w} M$$

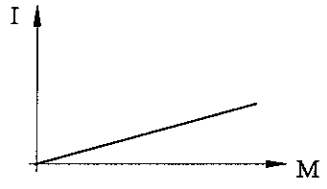

Figure 1.28.

Therefore the generated torque M is directly proportional to the motor current I. A further important characteristic quantity is the specific torque $k_M$ , which can be determined from Eq. 1.29.

Eq. 1.31 $$k_M = \frac{M}{I} = \frac{4}{\pi^2} B_o r \ell w$$

We can consider the loss torque $M_V$ developed within the motor in Eq. 1.29 by substituting $M = M_b + M_V$ for the generated torque ($M_b$ = Motor output load torque).
For $M_b = 0$, therefore $M = M_{Vo}$ and Eq. 1.30 renders the no load current $I_o$ of the motor

Eq. 1.32 $$I_o = \frac{\pi^2}{4} \frac{1}{B_o r \ell w} M_{Vo}$$

Since $B_0$ falls off slightly at the air gap end, but we calculated using the maximum value, the actual current will be slightly greater than that predicted by Eq. 1.30. We can consider this by correcting the $B_0$ with an empirically determined factor $c_1<1$.

### 1.7.2. Rotational Speed

As demonstrated in section 1.1, on one hand a current carrying conductor is exposed to a force when placed in a magnetic field on the other hand an emf is induced on a conductor moving in a magnetic field. The following holds for this motion induced emf

Eq. 1.33 $e_i = \int [\mathbf{v} \times \mathbf{B}] \cdot d\ell$

Adapted to the internal motor relationships, that is induction **B** perpendicular to the direction of motion **v** and also perpendicular to conductor length $\ell$, the result for the induced emf on one conductor is

Eq. 1.34 $e_i = v\,B\,\ell$

At constant circumferential speed v and design required conductor length $\ell$ therefore the instantaneous value of the induced voltage e is a direct image of the induction curve B.
The summation of all induced voltage components from the individual winding segments generates the well known back emf, which is proportional to rotational speed and opposite of the applied voltage U.
With this, one can replace the motor with a simplified equivalent circuit diagram as follows:

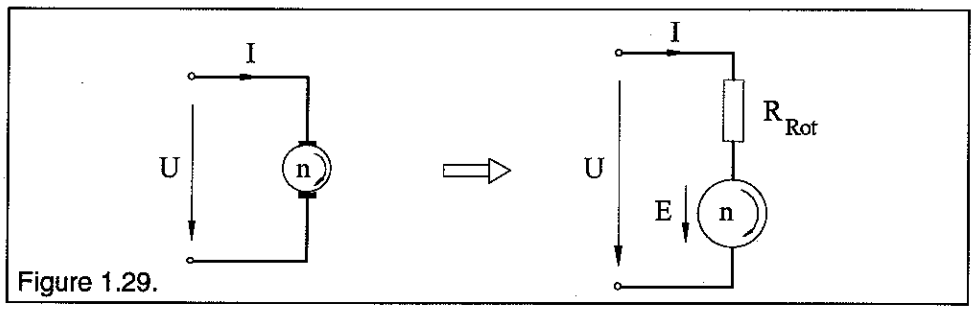

Figure 1.29.

In order to generate the required torque M in a motor we require the current I as calculated with Eq. 1.30. If we represent the winding resistance as $R_{Rot}$ between the connection tabs than we can solve for the current with the simultaneous equations

Eq. 1.35 $U - E - IR_{Rot} = 0$

Eq. 1.36 $I = \dfrac{U - E}{R_{Rot}}$

By setting Eq. 1.30 and Eq. 1.36 equivalent to I we get

Eq. 1.37 $\dfrac{\pi^2}{4}\dfrac{1}{B_o r \ell w} M = \dfrac{U - E}{R_{Rot}}$

To get the rotational speed as a function of torque n(M) we must clearly solve for the dependency of induced voltage on rotational speed E(n) next.

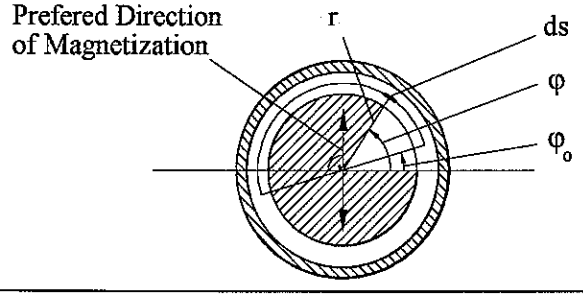


Figure 1.30.

We identify the orientation of a rhomb as in Figure 1.30 unwound into a plane as in Figure 1.31..

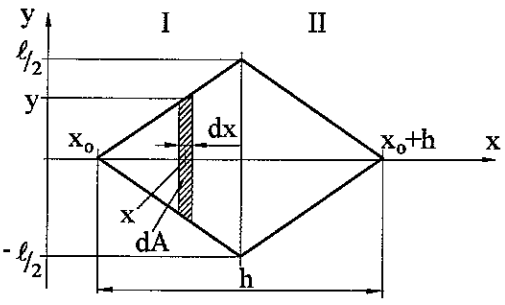


Figure 1.31.

By moving this rhomb a voltage $e_i$ is induced according to the induction law

Eq. 1.38 $$e_i = -\frac{d\Phi}{dt} = -\frac{d}{dt}\int_A \mathbf{B}\cdot d\mathbf{A}$$

Next we will determine the force flow, which goes perpendicular through the rhomb,

Eq. 1.39 $$\Phi = \int_A \mathbf{B}\cdot d\mathbf{A} = \iint B\,dxdy$$

determine and assume that B is constant in the axial direction and thereby independent of y. The integration over dy yields 2y. This results in the flux

Eq. 1.40 $$\Phi = \int B2ydx$$

As we can see in Figure 1.31 , in the rhomb half I

Eq. 1.41 $$y = \frac{\ell}{h}(x - x_o)$$

holds specifically with $x = r\varphi$, $x_0 = r\varphi_0$, $h = r\pi$

Eq. 1.42 $y = \frac{\ell}{\pi}(\varphi - \varphi_o)$ for $\varphi_0 \le \varphi \le \varphi_0 + \pi/2$

In rhomb half II we have

Eq. 1.43 $y = -\frac{\ell}{\pi}(\varphi - \varphi_o - \pi)$ for $\varphi_0 + \pi/2 \le \varphi \le \varphi_0 + \pi$

From Eq. 1.40, Eq. 1.42 and the relationship $B = B_o \sin\varphi$ as well as $dx = r d\varphi$ the flux through rhomb half II is

Eq. 1.44 $$\Phi_I = \frac{2}{\pi} B_o \ell r \int_{\varphi_o}^{\varphi_o + \pi/2} (\varphi - \varphi_o) \sin\varphi \, d\varphi =$$

$$= \frac{2}{\pi} B_o \ell r \left[\sin\varphi - \varphi\cos\varphi + \varphi_o \cos\varphi\right]_{\varphi_o}^{\varphi_o + \pi/2}$$

Eq. 1.45 $$\Phi_I = \frac{2}{\pi} B_o \ell r \left(\cos\varphi_o - \sin\varphi_o + \frac{\pi}{2}\sin\varphi_o\right)$$

For the flux through II we get according to Eq. 1.43

Eq. 1.46 $$\Phi_{II} = -\frac{2}{\pi} B_o \ell r \int_{\varphi_o + \pi/2}^{\varphi_o + \pi} (\varphi - \varphi_o - \pi) \sin\varphi \, d\varphi =$$

$$= -\frac{2}{\pi} B_o \ell r \left[\sin\varphi - \varphi\cos\varphi + (\varphi_o + \pi)\cos\varphi\right]_{\varphi_o + \pi/2}^{\varphi_o + \pi}$$

Eq. 1.47 $$\Phi_{II} = \frac{2}{\pi} B_o \ell r \left(\cos\varphi_o + \sin\varphi_o - \frac{\pi}{2}\sin\varphi_o\right)$$

for the entire flux through the rhomb $\Phi = \Phi_I + \Phi_{II}$ we get with Eq. 1.45 and Eq. 1.47

Eq. 1.48 $$\Phi = \frac{4}{\pi} B_o \ell r \cos\varphi_o$$

From the law of induction we get the induced voltage in the rhomb as

Eq. 1.49 $$e_{iR} = -\frac{d\Phi}{dt} = -\frac{4}{\pi} B_o \ell r \frac{d}{dt}\cos\varphi_o$$

If the spool is rotating with angular velocity $\omega = d\varphi/dt$, then, if we let the time base line t begin when our specific wire rhomb is at $\varphi_0 = 0$, $\varphi_0 = \omega t$ and therefore

Eq. 1.50 $$e_{iR} = \frac{4}{\pi} B_o \ell r \omega \sin\omega t$$

At this time we will compare the induced voltage in the rhomb to that of a single, parallel to the axis of rotation conductor of length $\ell_D$. The relative angular

orientation of the conductor with respect to the rhombs peak is defined as angle $\beta$.
With $v = r\omega$, $B = B_0 \sin\varphi$ and $\varphi = \varphi_0 + \beta$ we get with Eq. 1.34

Eq. 1.51 $$e_{iD} = v\,B\,\ell_D = r\,\omega B_o \ell_D \sin\varphi = B_o \ell_D r\,\omega \sin(\varphi_o + \beta)$$

Here too we let the time base line begin at $\varphi_O = 0$, therefore $\varphi_O = \omega t$

Eq. 1.52 $$e_{iD} = B_o \ell_D r\,\omega \sin(\omega t + \beta)$$

Because $\sin(\alpha + \beta) = \sin\alpha\cos\beta + \cos\alpha\sin\beta$ we get for $\beta = 0$

Eq. 1.53 $$e_{iD} = B_o \ell_D r\,\omega \sin\omega t$$

We will now arrange the conductor according to Figure 1.8, so two diametrically arranged, straight conductor segments connected to form one winding (the connecting wire does not affect the induced voltage, it only raises the resistance). Hereby we double $e_{iD}$, so we get the value of Eq. 1.53 times two. To get the same induced voltage as in a single rhomb we could form the winding so the straight segments have $\ell_D = \ell 2/\pi$ , therefore shorten the spool by the factor $2/\pi$. This follows from

Eq. 1.54 $$e_{iR} = e_{iD} = \frac{4}{\pi} B_o \ell\, r\,\omega \sin\omega t = 2\,B_o \ell_D r\,\omega \sin\omega t$$

Because of the requirement $\beta = 0$ the straight conductor segments must be aligned with the rhombs peak at $\varphi = 0$ and $\varphi = \pi$, to get the same phase relationship.

We now return to calculating the voltage induced in the winding. Again we will idealize the commutator with very fine segments and continuous cyclic wire changing. Then a circumferential linear element ds will constantly be in the position $\varphi_O = \omega t$ in which there are $v\,ds = v\,r\,d\varphi_O$ rhombs, of which each has an induced voltage $e_{iR}$ according to Eq. 1.50. In the linear element ds the total voltage

Eq. 1.55 $$dE = \frac{4}{\pi} B_o \ell\, r^2 v\,\omega \sin\varphi_o\, d\varphi_o$$

will be induced. By integrating dE of all the rhombs in the interval $0 \le \varphi_O \le \pi$ we will get the total voltage induced in the rotor (Since the rotor segments between the intervals $0 \le \varphi_O \le \pi$ and $\pi \le \varphi_O \le 2\pi$ are connected in parallel between the brushes, we can only integrate over one interval). We get from Eq. 1.55

Eq. 1.56 $$E = \frac{4}{\pi} B_o \ell\, r^2 v\,\omega \int_0^{\pi} \sin\varphi_o\, d\varphi_o =$$

$$= \frac{4}{\pi} B_o \ell\, r^2 v\,\omega \left[-\cos\varphi_o\right]_0^{\pi} =$$

Eq. 1.57 $$= \frac{8}{\pi} B_o \ell\, r^2 v\,\omega$$

and further with $\nu = w/2r\pi$ as well as $\omega = 2\pi n$

Eq. 1.58 $$E = \frac{8}{\pi} B_o \ell r w n$$

With this we substitute as planned into Eq. 1.37 and get the dependance of rotational speed n and torque M as follows:

Eq. 1.59 $$n = \frac{\pi}{8} \frac{U}{B_o \ell r w} - \frac{\pi^3}{32} \frac{R_{Rot}}{(B_o \ell r w)^2} M$$

If we substitute the specific torque $k_M$ from Eq. 1.31 we get

Eq. 1.60 $$n = \frac{1}{2\pi} \left( \frac{U}{k_M} - \frac{R_{Rot}}{k_M^2} M \right)$$

With this linear equation we can determine the axis intersection on coordinate system n(M).
For the case when M = 0, this is a completely unloaded motor with zero loss torque $M_V$, we get the so called ideal no load speed $n_i$

Eq. 1.61 $$n_i = \frac{1}{2\pi} \frac{U}{k_M}$$

and with n = 0, this is a locked rotor motor, we get the so called ideal stall torque $M_{iH}$

Eq. 1.62 $$M_{iH} = \frac{U}{R_{Rot}} k_M$$

Neither ideal no load speed $n_i$ nor ideal stall torque $M_{iH}$ can be realized. In either case the loss moment $M_V$ will cause a corresponding reduction
Now we can graphically show the dependency of rotational speed n and torque M at a constant voltage U.

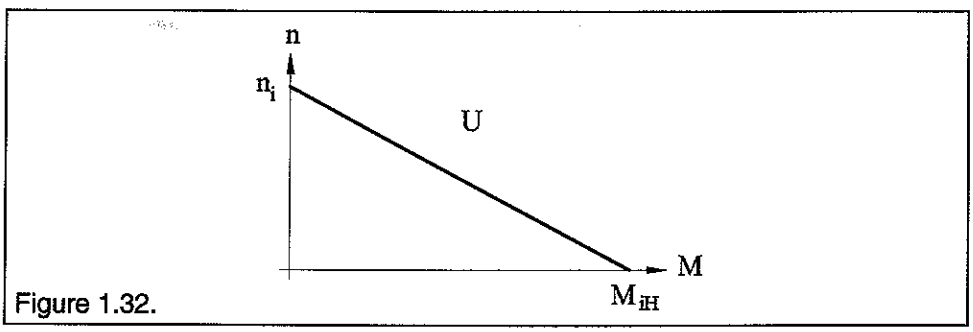

Figure 1.32.

With the parameters $n_i$ and $M_{iH}$ we can define the slope $\Delta n / \Delta M$ of the characteristic line as the speed/torque gradient.

Eq. 1.63 $$\frac{\Delta n}{\Delta M} = \frac{n_i}{M_{iH}} = \frac{1}{2\pi} \frac{R_{Rot}}{k_M^2}$$

with this we can transform Eq. 1.60 into

$$\text{Eq. 1.64}\quad n = n_i\left(1-\frac{M}{M_{iH}}\right) = n_i - \frac{\Delta n}{\Delta M}M$$

Setting $M = M_{V0}$, that is loss torque is the only load, we get the effective no load rotational speed as $n_0$

$$\text{Eq. 1.65}\quad n_o = n_i - \frac{\Delta n}{\Delta M}M_{Vo}$$

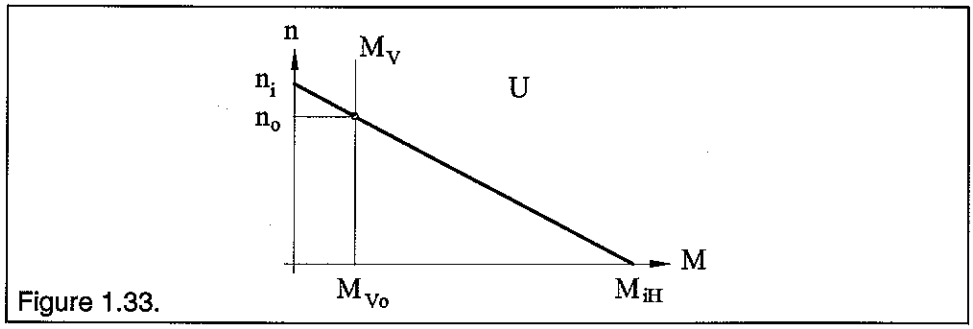

Figure 1.33.

Since $R_{Rot}$ increases with rising temperature, the ideal stall torque $M_{iH}$ will decrease as we can recognize from Eq. 1.62 and will increase, therefore worsen the speed/torque gradient $\Delta n / \Delta M$. For application required load torque $M_b$ the reduction of load speed due to temperature rise is insignificant. For dynamic operation the motor will operate on a slightly steeper speed/torque gradient.

Because of these relationships the applications with rising temperature $\Theta$ will result in a set of characteristic lines for constant voltage U. For temperature < $\Theta_1 < \Theta_2 < \Theta_3 < \Theta_4$ holds.

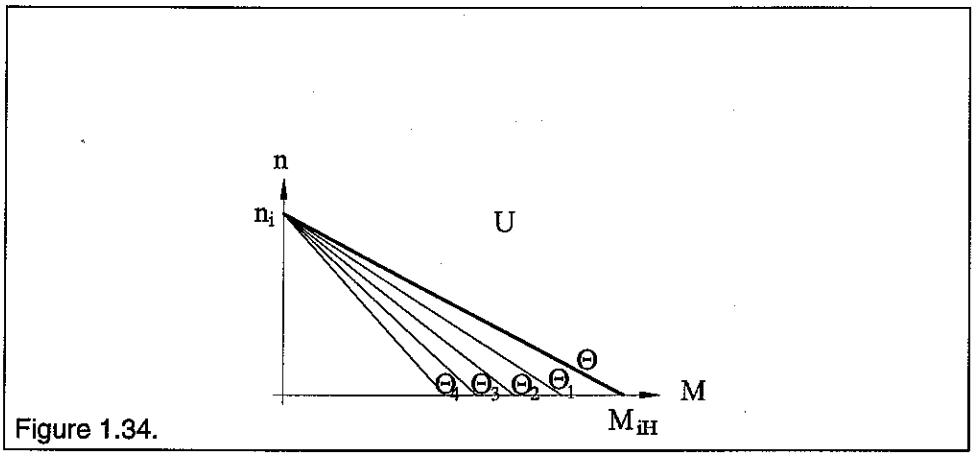

Figure 1.34.

Because temperature rises as load increases the motor is limited to a maximum operating torque $M_{zul}$. At this torque the rotor approaches its ultimate temperature assuming a surrounding temperature of 25 °C. If heat transfer is improved, naturally, the maximum operating torque can be increased, on the other hand if the surroundings are warmer then the maximum torque must be reduced.

### 1.7.3. Starting Process

If we define the rotors moment of inertia as $J_R$, then its equation of motion with the relationship $\omega = 2\pi n$ is

Eq. 1.66 $$M_B = J_R \frac{d\omega}{dt} = 2\pi J_R \frac{dn}{dt}$$

For the starting process the acceleration moment $M_B$ consists of $M_B = M - M_V - M_b$. Loss moment $M_V$ and load torque $M_b$ reduce the generated torque M.

Integrating Eq. 1.66 we get the time required to reach a specified rotational speed n from n = 0.

Eq. 1.67 $$t = 2\pi J_R \int_0^n \frac{dn}{M_B}$$

If we simplify the no load start by setting $M_V = 0$, then $M_B = M$, and we get with Eq. 1.64

Eq. 1.68 $$M_B = M = (n_i - n)\frac{M_{iH}}{n_i}$$

and therefore

Eq. 1.69 $$t = 2\pi J_R \frac{n_i}{M_{iH}} \int_0^n \frac{dn}{(n_i - n)} = 2\pi J_R \frac{n_i}{M_{iH}} \left[-\ln(n_i - n)\right]_0^n$$

we define a mechanical time constant $\tau_m$

Eq. 1.70 $$\tau_m = 2\pi J_R \frac{n_i}{M_{iH}} = 2\pi J_R \frac{\Delta n}{\Delta M} = J_R \frac{R_{Rot}}{k_M^2}$$

Then by substituting the limits of integration

Eq.1.71 $$-\frac{t}{\tau_m} = \ln \frac{n_i - n}{n_i}$$

or appropriately rewritten the idealized development of rotational speed during the starting process

Eq.1.72 $$n = n_i\left(1 - e^{-\frac{t}{\tau_m}}\right)$$ in reality we have $$n = n_o\left(1 - e^{-\frac{t}{\tau_m}}\right)$$

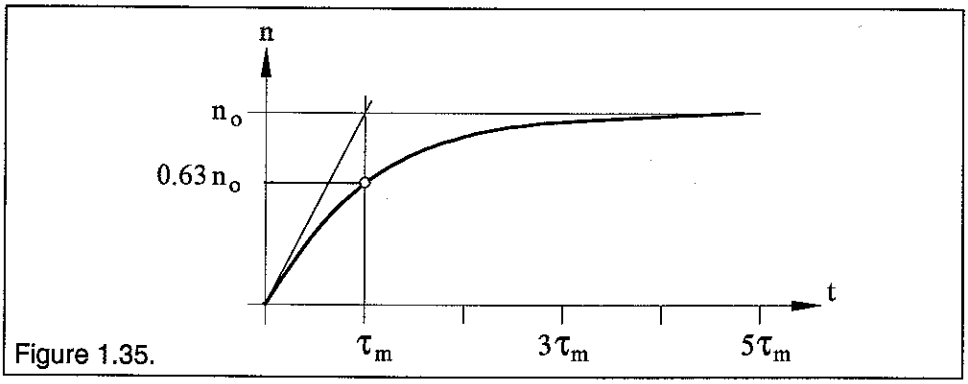

Figure 1.35.

So we see, after the motor is turned on, that the rotational speed increases according to an exponential function. Naturally the ideal no load speed can never be attained. The output torque will always be reduced by the loss torque $M_V$. The motor therefore only accelerates to the no load speed $n_o$. For $t = \tau_m$ $n = 0{,}63n_o$, or after $t = 3\tau_m$ $n = 0.95n_o$ is reached, therefore the starting process is practically over within three mechanical time constants.
Since the mass of the rotors in the **maxon**-Motor program are primarily made up off the winding their moment of inertia $J_R$ and corresponding mechanical time constants $\tau_m$ are very small, $\tau_m$ is in the range of 0.004 to 0.035 seconds.

In practice the case of a motor accelerating unloaded occurs rarely. Usually the motor is connected to its load with a drive element, be it pulley or pinion, which add a further moment of inertia $J_b$.
For practical starting processes the entire moment of inertia $J = J_R + J_b$ applied to the motor shaft must be considered. The mechanical time constant is then calculated from the motor plus load

Eq.1.73 $$\tau_{mges} = (J_R + J_b)\,2\pi\frac{n_i}{M_{iH}}$$

or substituting the motor time constant $\tau_m$ and simplifying

Eq.1.74 $$\tau_{mges} = \tau_m\left(1+\frac{J_b}{J_R}\right)$$

adding a moment of inertia so $J_b = J_R$ will double the mechanical time constant of the system.

### 1.7.4. Power

If we want to determine the motor's power output P we can start with several known properties of mechanics.
Work $W_{mech}$ is defined as the integral of a force F along a distance s

Eq.1.75 $$W_{mech} = \int_0^s \mathbf{F}\cdot d\mathbf{s}$$

Similarly we can define work $W_{mech}$ performed by a rotating shaft as the integral of the torque $M_b$ along the angle $\varphi$

Eq.1.76 $W_{mech} = \int_0^{\varphi} M_b d\varphi$

Since power P is defined as work per unit time we have for our rotating case

Eq.1.77 $P_{mech} = \frac{dW_{mech}}{dt} = \frac{d}{dt}\int_0^{\varphi} M_b d\varphi$

and if we assume constant motion ($d\varphi/dt = \omega = 2\pi n$ = constant ) with constant torque $M_b$ the familiar equation results

Eq.1.78 $P_{mech} = M_b \omega = M_b 2\pi n$

If we divide torque M into loss torque $M_V$ and load torque $M_b$ in other words M = $M_b$ + $M_V$ , then we get

Eq.1.79

$$P = P_{mech} = M_b 2\pi n = 2\pi n_i (1 - \frac{M}{M_{iH}}) M_b = 2\pi n_i \frac{M_{iH} - M_b - M_V}{M_{iH}} M_b$$

Eq.1.80 $$P = 2\pi n_i \frac{(M_{iH} - M_V) M_b - M_b^2}{M_{iH}}$$

If we assume loss torque $M_V$ to be a constant than the the so called power parabola can be graphed as follows

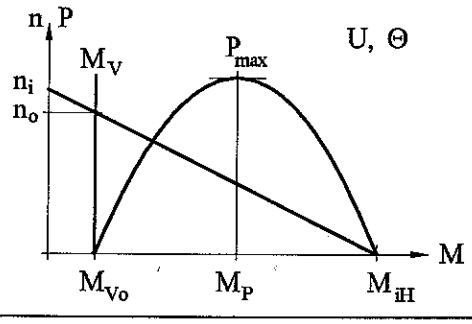


Figure 1.36.

The maximum of this quadratic equation can be found by setting the first differential equal to zero

Eq.1.81 $$\frac{dP}{dM_b} = 2\pi n_i \frac{M_{iH} - M_V - 2M_b}{M_{iH}} = 0$$

The result is the value of load torque $M_P$ at maximum power output

Eq.1.82 $$M_P = \frac{M_{iH} - M_V}{2}$$

Substituting into Eq.1.80 we get the maximum power output as reduced by the winding's temperature rise

Eq.1.83 $$P_{max} = \frac{\pi}{2} n_i \frac{(M_{iH} - M_V)^2}{M_{iH}}$$

In actual applications the motor can only be operated at its maximum power output if the load torque in $M_b$ does not exceed the limit of $M_b \leq M_{zul} = k_M$ (see 1.7.7.2).

### 1.7.5. Efficiency

Efficiency $\eta$, by definition, is the relationship between power input $P_{zu}$ and power output P. For a perfect frictionless, loss less machine the efficiency $\eta = 1$ follows from the equality $P = P_{zu}$. In reality things look less favorable. This will be explained, in simplified terms, in the following derivation.

Eq.1.84 $$\eta = \frac{P}{P_{zu}}$$

We can substitute Eq. 1.80 for power output P and UI for power input $P_{zu}$ = UI. Then for efficiency we have $\eta$

Eq.1.85 $$\eta = \frac{P}{P_{zu}} = \frac{2\pi n_i}{UI} \frac{(M_{iH} - M_V)M_b - M_b^2}{M_{iH}}$$

The substitutions Eq.1.61 for $n_i$ and Eq.1.30 for I, and $M = M_b + M_V$, yields efficiency $\eta$ as a function of load torque $M_b$

Eq.1.86 $$\eta = \frac{(M_{iH} - M_V)M_b - M_b^2}{(M_b + M_V)M_{iH}}$$

The general shape of the efficiency curve is depicted in Figure 1.37. The curve shows a pronounced maximum, which we will derive mathematically.

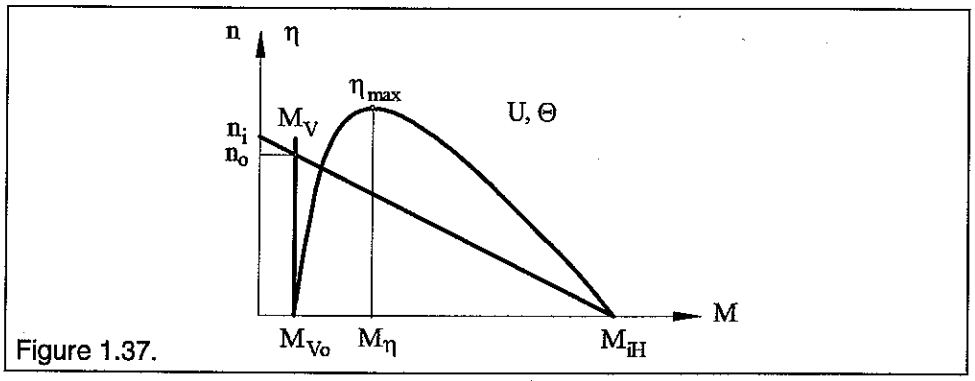


Figure 1.37.

We find the maximum efficiency by setting the first derivative of the efficiency equation equal to zero as follows

Eq.1.87 $$\frac{d\eta}{dM_b} = 0$$

By applying the rule of quotients to the efficiency equation we get

Eq.1.88 $M_b^2 + 2M_V M_b + (M_V^2 - M_V M_{iH}) = 0$

The general solution to this quadratic equation results in the desired torque $M_\eta$, where maximum efficiency $\eta_{max}$ occurs

Eq.1.89 $M_\eta = M_{b1,2} = -M_V \pm \sqrt{M_V M_{iH}}$

Only the positive result is of physical significance therefore

Eq.1.90 $M_\eta = -M_V + \sqrt{M_V M_{iH}}$

With this the equation for maximum efficiency $\eta_{max}$ becomes

Eq.1.91 $$\eta_{max} = \frac{(M_{iH} - M_V)M_\eta - M_\eta^2}{(M_\eta + M_V)M_{iH}}$$

After substituting for $M_\eta$ and several intermediate calculations we get the maximum efficiency $\eta_{max}$ with the simplifying assumptions of rotational speed independent loss torque $M_V = M_{Vo}$ and negligible effects due to winding temperature rise $\Theta$ (both effects reduce the efficiency but are usually negligible in practice)

Eq.1.92 $$\eta_{max} \approx \left(1 - \sqrt{\frac{M_V}{M_{iH}}}\right)^2 = \left(1 - \sqrt{\frac{I_o}{I_H}}\right)^2$$

As we can see from the equation the quotient of ideal stall torque $M_{iH}$ and loss torque $M_V$ determines maximum efficiency $\eta_{max}$. Thus for any given motor, with its loss torque predefined by design, the maximum theoretical efficiency can be improved by increasing the applied voltage U as determined by the relationship $M_{iH} = Uk_M / R_{Rot}$.

### 1.7.6. Characteristic Line Description

If we graph the derivation thus far on common axes we get the characteristic lines of a DC motor with self supported winding. The parameters winding temperature $\Theta_R$, Voltage U and loss torque $M_V$ are assumed to be constants.

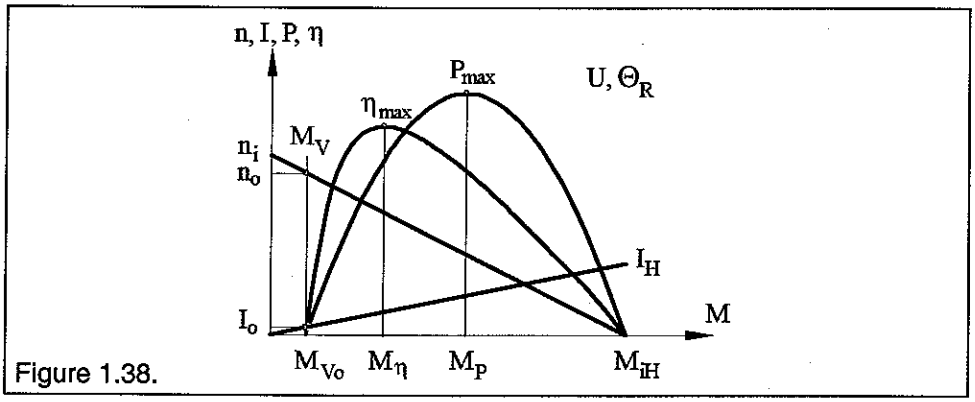


Figure 1.38.

### 1.7.7. Thermal Characteristics

The internal losses $P_V$ consist of two main components which, depending on operating point, will vary in relative magnitude. For small loads, generally the dominating component will be frictional losses $P_R = M_V\omega$ , at higher loads Joule's or electric heat losses $P_J = I^2 R_\Theta$., which are noticeable as mechanical vibrations or noises, can be added to the frictional losses, for the purposes of our basic discussion.

Eq.1.93 $P_V = P_R + P_J = M_V\omega + I^2R_\Theta$

#### 1.7.7.1. Maximum Power Dissipation

The heat transfer from the motor to the surrounding air occurs through three different heat transfer mechanisms simultaneously. The mechanisms are differentiated as conducting, convecting and radiating.

Characterizing heat conduction is the coefficient of thermal conductivity $\lambda$, which is approximately 100 times greater in magnitude for metals when compared to insulators. The energy flow is proportional to the product of $\lambda\ \Delta\Theta$ d ($\Delta\Theta$ = difference of the absolute temperatures).
Convection is described by the coefficient of thermal transmission $\alpha$, which is dependant upon the specific heat and state of motion of the surrounding fluid (carrier). The energy flow is proportional to the product of $\alpha\ \Delta\Theta$ A ($\Delta\Theta$ = difference of the absolute temperatures).
Radiation is characterized by the coefficient of thermal radiation $C_S$, which is based upon a black body. The energy flow is proportional to the product of($\Theta_K^4 - \Theta_U^4$)A ($\Theta_K$ and $\Theta_U$ are expressed as absolute temperatures).

The actual contribution of each of the three mechanisms to the total heat transfer depends upon surroundings and operating point. Any equation we can derive will therefore be greatlty limited to a generally valid rotational speed and temperature independant form. For example heat transfer due to radiation is practically negligible at temperature differences of less than 100°C, but becomes more effective above that point. Likewise there is practically no convection when the motor is stopped and thereby its contribution becomes negligible. Conversely as rotational speed increases a real increase in convection follows with an increase in the coefficient of thermal transmission $\alpha$.

To simplify the mathematical model the three mechanisms of heat transfer can be combined into one thermal resistance. We can construct an analgous electric circuit with resistance $R_{th}$, temperature differential $\Delta\Theta$ and heat current $P_V$:

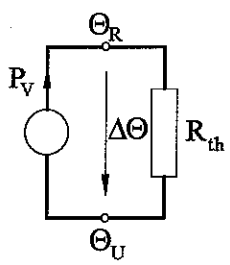


Figure 1.39.

Eq.1.94 $\Delta\Theta = P_V R_{th} = \Theta_R - \Theta_U$

Adapting the equation for the requirements of a motor we use the maximum permissable winding temperature $\Theta_{Rmax}$. Taking ambient temperature $\Theta_U$ into account the following equation results for maximum power dissipation $P_{Vzul}$

Eq.1.95 $\Delta\Theta = \Theta_{R\,max}\Theta_U = P_{Vzul}R_{th}$

Eq.1.96 $P_{Vzul} = \frac{\Delta\Theta}{R_{th}} = \frac{\Theta_{R\,max} - \Theta_U}{R_{th}}$

In the previous discussion the entire thermal resistance $R_{th}$ between motor and surroundings was used. Required by design the rotor is housed in a stator, therefore the heat loss is transmitted first to the stator then to the surroundings. Therefore we can divide thermal resistance $R_{th}$ into internal and external components. The heat transfer between rotor and stator will comprise the internal thermal resistance $R_{th1}$ and between stator and environment the external thermal resistance $R_{th2}$.

Eq.1.97 $R_{th} = R_{th1} + R_{th2}$

External thermal resistance can be reduced by relatively simple means (cooling fins, metal mounting, forced cooling) allowing an increased operating load strictly from a temperature point of view.
With the temperature rise characterisitcs and a stationary operating motor we obtain the maximum power dissipation $P_{Vzul}$ dissipation as

Eq.1.98 $P_{Vzul} = \frac{\Theta_{R\,max} - \Theta_U}{R_{th1} + R_{th2}}$

With this we can construct a more accurate analgous electric circuit for heat transfer by using stator, or housing, temperature $\Theta_S$

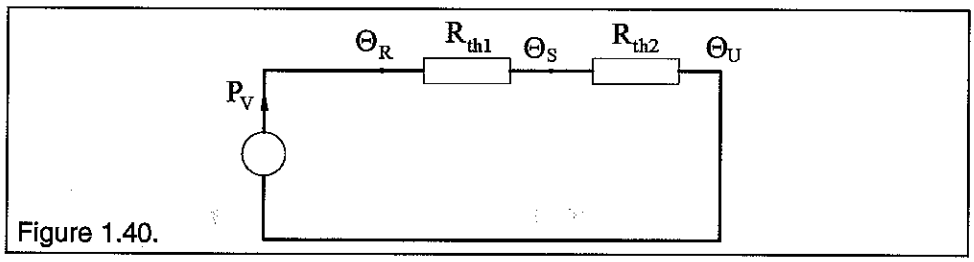

Figure 1.40.

and approximate the gauging temperatures

Eq.1.99 $\Theta_S = \Theta_U + P_V R_{th2}$

Eq.1.100 $\Theta_R = \Theta_U + P_V(R_{th1} + R_{th2})$

### 1.7.7.2. Maximum Load Current

As we saw during the study of efficiency the power input $P_{zu}$ is the sum of power loss $P_V$ and power output P.

Eq.1.101 $P_{zu} = P_V + P$

Using efficiency $\eta$ calculated at any random operating point P the power losses $P_V$ ,manifested as heat, can be calculated from

Eq.1.102 $$P_V = P_{zu} - P = \left(\frac{P_{zu}}{P} - 1\right) P = \frac{1-\eta}{\eta} P$$

As can be easily recognized the power losses $P_V$ increase with increasing power output P, but must be limited due to the maximum permissable motor temperature rise.

To further clarify we examine two limiting cases. With a locked rotor or time t = 0 during start up there is no power output, all power in $P_{zu}$ is converted to Joule's losses $P_J$ u ( $P_{zu} = P_J = I^2 R_\Theta$). Since there is no motion there are obviously no frictional losses. The other limiting case is the no load condition. In this case, as before, there is no power output P, instead the power input $P_{zu}$ is converted to Joule's $P_J$ and frictional $P_R$ losses
( $P_{zu} = P_R + P_J = M_V \omega_0 + I^2 R_\Theta$ ).

For this discussion the most interesting point, where the motor reaches its maximum temperature, lies somewhere between these limits. For a simplified, but valid for most cases, calculation we will neglect the frictional losses $P_R$ and concentrate only on Joule's losses $P_J$. this yields the following simplified relationship

Eq.1.103 $$P_{Vzul} = P_J = I_{zul}^2 R_{\Theta max}$$

the temperature dependance of resistance R can be shown in the familiar form of

Eq.1.104 $$R_\Theta = R_{25}[1 + \alpha_{Cu}(\Theta - 25)] \quad \text{bzw.}$$
$$R_{\Theta max} = R_{25}[1 + \alpha_{Cu}(\Theta_{R max} - 25)]$$

From these equations we solve for the maximum permissable load current $I_{zul}$

Eq.1.105 $$I_{zul} = \sqrt{\frac{P_{Vzul}}{R_{\Theta max}}}$$

or with respect to thermal resistances and temperatures

Eq.1.106 $$I_{zul} = \sqrt{\frac{\Theta_{R max} - \Theta_U}{(R_{th1} + R_{th2}) R_{\Theta max}}}$$

As can be deduced, the effect of increasing the maximum permissable winding temperature $\Theta_{Rmax}$ is greater on the maximum permissable load current $I_{zul}$ than is lost through the requisite increases in winding impedance $R_{\Theta max}$.

### 1.7.7.3. Warming and Thermal Time Constants

During previous discussions we assumed steady state warming processes. For our continuing study we want to determine the temperature change of stator and rotor with respect to time. Part of power dissipation $P_V$ developed during time interval dt will be absorbed by the rotor as a temperature rise, the balance will be transferred to the stator. The sum of generated heat, transmitted heat and stored heat must, of course, be zero. As we will see the heat capacity of the rotor is a fraction of the stators. To simplify the calculation we can assume

the stators temperature to be a constant. With that we can start to define thermal equilibrium as follows:

Eq.1.107 $$P_V dt - \frac{\Theta_R - \Theta_S}{R_{th1}} dt - C_R d\Theta = 0$$

Where we introduce the parameter for thermal capacity $C_R = m_R c_R$ of the rotor

Eq.1.108 $$R_{th1} C_R \frac{d\Theta_R}{dt} + \Theta_R - \Theta_S - P_V R_{th1} = 0$$

With that we obtain the first order non-homogeneous differential equation for rotor temperature $\Theta_R$

Eq.1.109 $$R_{th1} C_R \frac{d\Theta_R}{dt} + \Theta_R = \Theta_S + P_V R_{th1}$$

which can be solved in two steps. A particular solution of the non-homogeneous differential equation can be determined immediately as

Eq.1.110 $$\Theta_{Rp} = \Theta_S + P_V R_{th1}$$

We solve the non-homogeneous differential equation for $\Theta_{Rh}$ by seperating the variables and subsequent integration.

Eq.1.111 $$R_{th1} C_R \frac{d\Theta_{Rh}}{dt} + \Theta_{Rh} = 0$$

Eq.1.112 $$\frac{d\Theta_{Rh}}{\Theta_{Rh}} = -\frac{1}{R_{th1} C_R} dt$$

Eq.1.113 $$\ln \Theta_{Rh} - \ln c_e = -\frac{1}{R_{th1} C_R}$$

We define the fraction's denominator as the thermal time constant $\tau_{th1}$ for the following derivations.

Eq.1.114 $$\tau_{th1} = R_{th1} C_R = R_{th1} m_R c_R$$

Following integration we get the solution for $\Theta_{Rh}$ of the non-homogeneous differential equation with a constant of integration $c_e$ yet to be determined.

Eq.1.115 $$\Theta_{Rh} = c_e e^{-\frac{t}{\tau_{th1}}}$$

The general solution follows familiarilly from a particular integral of the non-homogeneous differential equation and the solution of the homogeneous differential equation

Eq.1.116 $$\Theta_R = \Theta_{Rp} + \Theta_{Rh} = \Theta_S + P_V R_{th1} + c_e e^{-\frac{t}{\tau_{th1}}}$$

and with that for the sought function $\Theta_R$ the relationship

Eq.1.118 $$\Theta_R = \Theta_S + P_V R_{th1}\left(1 - e^{-\frac{t}{\tau_{th1}}}\right)$$

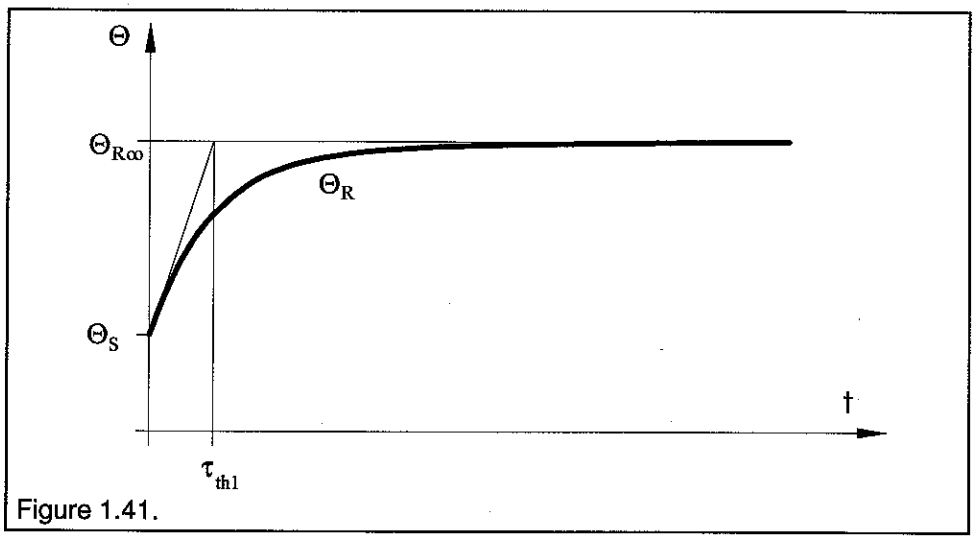

Figure 1.41.

For steady state, that is $t \rightarrow \infty$, we get the rotor temnperature $\Theta_R$

Eq.1.119 $$\Theta_{R\infty} = \Theta_S + P_V R_{th1}$$

Basically the same logic holds for the temperature rise in the stator. That is, the temperature rise occurs over time. The energy transferred from rotor to stator will be partially stored and the balance transferred to the environment.
Without going into an equivalent derivation we can state that, partially due to the much greater mass, the thermal time constant for the stator $\tau_{th2}$ is much greater than that for the rotor $\tau_{th1}$ ( $\tau_{th2} >> \tau_{th1}$ )

Eq.1.120 $$\tau_{th2} = R_{th2} C_S = R_{th2} m_S c_S$$

Generally $R_{th2} > R_{th1}$, but this can be altered through appropriate measure, (forced cooling, increasing heat emitting surface area with a heat sink).
The time dependant temperature rise is also an exponential function, although slowed significantly.

Eq.1.121 $$\Theta_S = \Theta_U + P_V R_{th2}\left(1 - e^{-\frac{t}{\tau_{th2}}}\right)$$

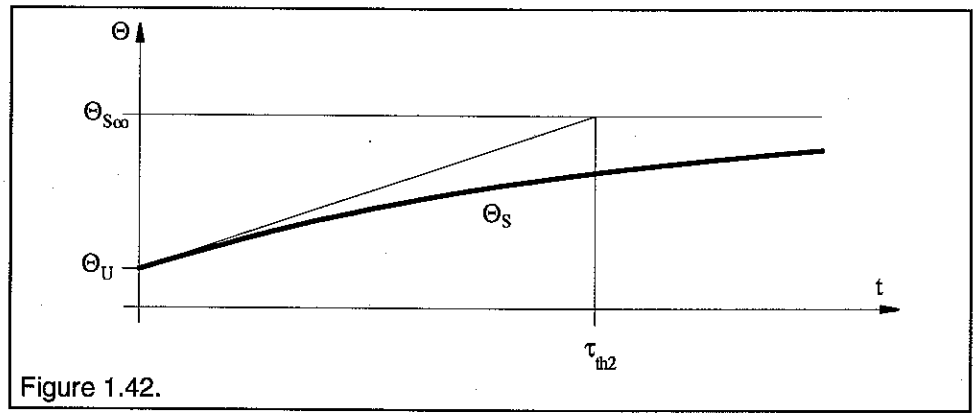

Figure 1.42.

For steady state, that is t $\rightarrow \infty$, we get the stator temperature $\Theta_S$

Eq.1.122 $$\Theta_{S\infty} = \Theta_U + P_V R_{th2}$$

In reality the temperautre rise in stator and rotor occur simultaneously, which can be seen in the approximate exponential curve. As is obvious from the two time functions of $\Theta_R$ and $\Theta_S$, monitoring stator temperature is much too slugish to effect thermal protection for the rotor.

### 1.7.7.4. Cooling

Similarily we can represent the cooling process mathematically. For a starting point we assume that the winding is at its maximum permissable temperature and there are no further power losses ( at $\Theta_{Rmax}$ and $P_V dt = 0$ ). The heat energy stored in the rotor at temperature $\Theta_{Rmax}$ is transferred to the stator at temperature $\Theta_S$. Under these conditions the heat equation appears as follows, assuming negligible stator cooling:

Eq.1.123 $$\frac{\Theta_R - \Theta_S}{R_{th1}} dt + C_R d\Theta_R = 0$$

We get a very similar $\tau_{th2}$ as the non-homogeneous differential equation of the warming process.

Eq.1.124 $$R_{th1} C_R \frac{d\Theta_R}{dt} + \Theta_R = \Theta_S$$

with a particular integral

Eq.1.125 $$\Theta_{Rp} = \Theta_S$$

The homogeneous differential equation is identical to that of the warming process

Eq.1.126 $$R_{th1} C_R \frac{d\Theta_{Rh}}{dt} + \Theta_{Rh} = 0$$

and the solution is of the same form

Eq.1.127 $$\Theta_{Rh} = c_a e^{-\frac{t}{\tau_{th1}}}$$

We again get the general solution form the sum of the two partial solutions

Eq.1.128 $$\Theta_R = \Theta_{Rh} + \Theta_{Rp} = \Theta_S + c_a e^{-\frac{t}{\tau_{th1}}}$$

and can determine the constant of integration $c_a$ with the starting points, that is at time t = 0 the rotor temperature is $\Theta_{Rmax}$. This yields

Eq.1.129 $$c_a = \Theta_{R\,max} - \Theta_S$$

and for the sought function of $\Theta_R$ we get the relationship

Eq.1.130 $$\Theta_R = \Theta_S \left( 1 - e^{-\frac{t}{\tau_{th1}}} \right) + \Theta_{R\,max} e^{-\frac{t}{\tau_{th1}}}$$

For steady state, that is $t \rightarrow \infty$, we get the rotor temperature, which can be verified with a simple substitution, as

Eq.1.131 $$\Theta_{R\infty} = \Theta_S$$

Adding the thermal capacities to the previously defined analogous electric circuit for heat transfer completes the circuit with respect to time. The following diagram results:

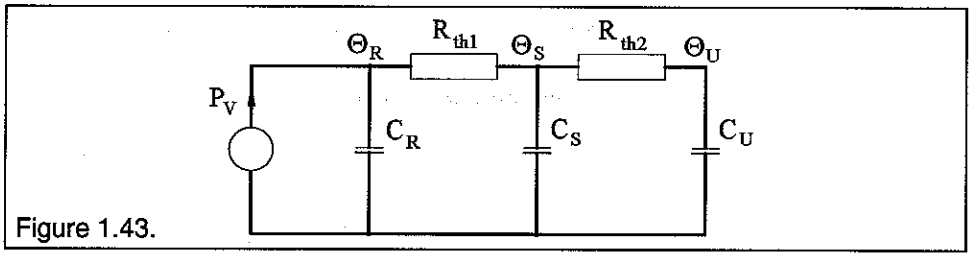


Figure 1.43.

The ambient thermal capacity $C_U$ approaches infinity since the motor, in most cases, will not affect the ambient temperature. As time approaches infinity, both thermal capacities $C_R$ and $C_S$ will be filled and their effect will disappear. With this we have a steady state condition, which is defined by our previous diagram.

### 1.7.7.5. Intermittent Use

Frequently motors operate in ON-OFF or intermittent use. Intermittent use is identified by continuously changing time segments $t_e$ with power dissipation $P_V$ and time segments $t_a$ without power dissipation. the motor's temperature rises during time $t_e$, and drops during time $t_a$. The cycle length is defined as $t_e + t_a = t_s$ and the ratio $t_e / t_s$ as relative on-off time. After a large number of cycles the temperature at the beginning and end of each cycle will be the same. We will define this moment as $t_n$. This is valid for both rotor and stator temperatures.
For the following diagram $t_e = (t_{n+2} - t_{n+1})$, $t_a = (t_{n+3} - t_{n+2})$ and for the whole cycle $t_s = (t_{n+3} - t_{n+1})$ is valid.

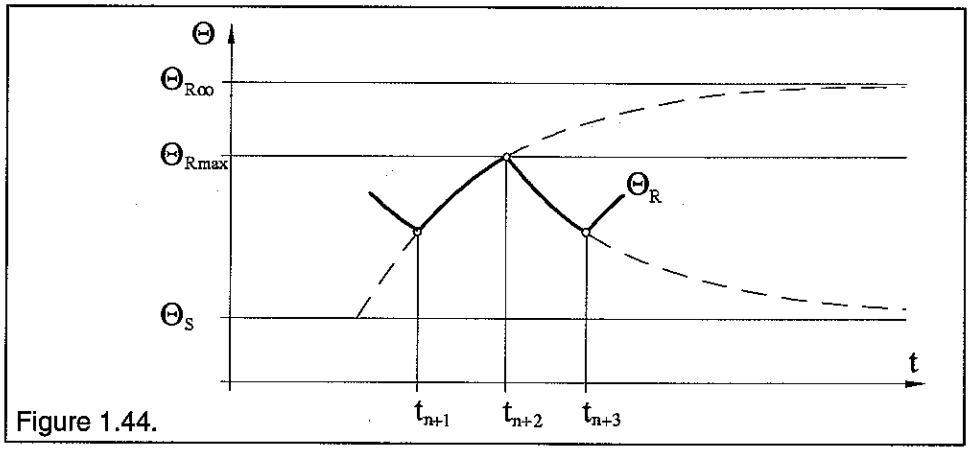

Figure 1.44.

If the cycle time $t_s$ is short with respect to the thermal time constant $\tau_{th}$, the temperature change during a single cycle is negligible. The temperature rise can then be determined as if a constant equivalent current where flowing. We can derive this from the following discussion:
Since the temperature change $\Delta\Theta = \Theta_{max} - \Theta_{min}$ during a single cycle $t_s$ can be viewed as negligible (of a higher order) we can replace $\Theta_{max}$ with an average temperature $\Theta_m$. The emitted power dissipation during cycle time $t_s$ must equal the sum of the individual power dissipations generated during each cycle segment $t_{ei}$ (other wise the temperature would rise or fall). This formulation is valid for any complicated cycle. If power dissipations $P_{V1}$, $P_{V2}$, .....$P_{Vn}$ are generated during cycle time segments $t_1$, $t_2$, .....$t_n$ (where individual $P_{Vi}$ could be zero), then we can write the equilibrium equation of emitted and generated power dissipation as

Eq.1.132
$$\frac{\Theta_m}{R_{th}}(t_1 + t_2 + ..... + t_n) = P_{V1}t_1 + P_{V2}t_2 + ..... + P_{Vn}t_n$$

Eq.1.133
$$\Theta_m = R_{th}\frac{P_{V1}t_1 + P_{V2}t_2 + ..... + P_{Vn}t_n}{(t_1 + t_2 + ..... + t_n)} = \frac{R_{th}\sum_{i=1}^{n} P_{Vi}t_i}{\sum_{i=1}^{n} t_i}$$

Since we are assuming that the power losses $P_{Vi}$ are generated as electric heat losses, the $P_{Vi}$ are proportional to the square of $I_i$. With this we can write the relationship for the average temperature as

Eq.1.134
$$\Theta_m \approx \frac{I_1^2t_1 + I_2^2t_2 + ..... I_n^2t_n}{t_1 + t_2 + ..... + t_n} = \frac{\sum_{i=1}^{n} I_i^2t_i}{\sum_{i=1}^{n} t_i}$$

in integral form with the instantaneous current of I this means nothing more than

Eq.1:135
$$\Theta_m \approx \frac{1}{T}\int_0^T i^2 dt = I_{eff}^2$$

For the case where cycle time $t_s$ is equal to or greater than the thermal time constant, the temperature rise calculations must be performed in single steps to ensure that the maximum permissible temperature is not exceeded.

# 2. Electronically Commutated DC Motors with Slotless Stator

## 2.1. Mode of Operation

The forces acting on current carrying conductors in a magnetic field we discovered in Section 1.2 can be applied in reverse according to the physical law action = reaction. The same effective forces, that are applied to the conductor by the magnet, are of course applied to the magnet by the conductor in opposite sense.
While the so called bell rotor motor has the winding rotating around the magnet between magnet and return path, the brushless motor has the winding attached to the stator and the rotor is the magnet mounted on the shaft.
Consequently the torque derived in section 1.3 can be adapted to the forces acting upon a rotatable permanent magnet.
A three phase **maxon**-EC-Motor (EC = electronic commutation) is also fitted with a rhombic winding permanently attached to a slotless stator. In order to generate a rotating magnetic field with the stator winding the winding must be separated into a minimum of three winding segments. Mechanical commutation is replaced with appropriate electronic switching circuits that provide current to the individual winding segments.
The identification of the relative angular position of the permanent magnet rotor is required for proper current supply to each winding segment. The **maxon**-EC-Motor determines the angular rotor position with three Hall sensors mounted 120° apart. The sensors scan a magnet ring that rotates with, and thereby defines the angular position of, the rotor.

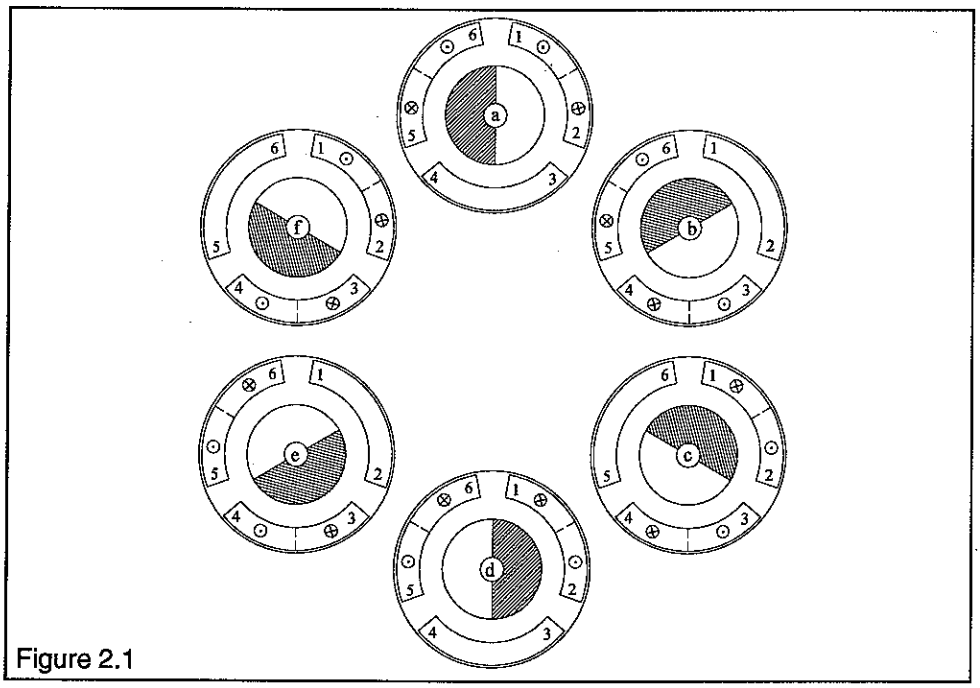

Figure 2.1

In the symbolic cross section of an EC-motor (Figure 2.1) it can be seen that the incremental rotating motion of the shaded rotor follows the advancing stator field in both rotational directions.
Two of the three spatially separated Y-connected stator windings become concurrently. The resulting field is dependant upon current flow direction and magnitude. Due to the combined effects of stator and rotor magnetic fields, the permanent magnet rotor attempts to align itself with the configuration of the stator field at hand.
As shown in Figure 2.1, six unique stator field distributions can be generated. A complete revolution of the rotor can therefore be divided into six steps of 60° each.

## 2.2. Design Principles

Building upon the well proven components of the mechanically commutated **maxon**-Motors, an equivalent, brushless design was realized. Figure 2.1 shows the sectional view of a **maxon** EC-Motor fitted with through shaft, ball bearings and rotor position sensors. As a rule **maxon** EC-Motors are equipped with RE-Magnets (RE = rare earth).

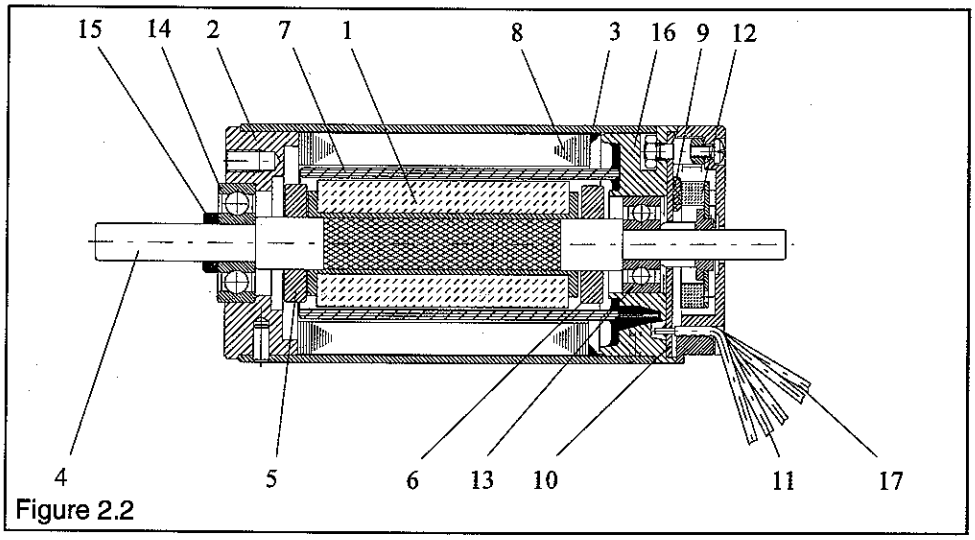

Figure 2.2

For **maxon**-EC-Motors the RE-Magnet (1) is mounted directly on the shaft (4) and, as a rotor, can be dynamically balanced with balancing rings (5) and (6), as required. The driving end of the shaft is located axially with a retaining ring (15). The two bearing flanges (2) and (16) together with the rust resistant steel sheath (3) and laminated slotless return path (8) form the supporting structure for the stator winding (7). A printed circuit board (10) provides connection between the winding taps and external wires (11). Hall sensors (9) mounted on PC board (10) sense a permanent magnet ring (12) rotating with the shaft (4) and furnish the rotor position information via control lines (17) to the drive electronics.

## 2.3. Magnet System

The fundamental discussion in section 1.4 of the optimum layout of the magnet system remain valid for **maxon**-EC-Motors. However there are several special considerations to keep in mind. The local magnetic flux in the stator is no longer constant with respect to time. Instead it changes cyclically with the rotation of the permanent magnet rotor. The resulting stator system losses will be

discussed in detail in the section "Iron Losses". To keep these losses within reason the magnetic flux carrying stator is constructed of laminated sheet metal rings. Imperfections in the material and mechanical asymmetry in the magnet system can lead to small detents.

## 2.4. Generating the Rotating Magnetic Field

As mentioned in section 2.1, the winding must have at least three spatially separated segments to enable generate a rotating magnetic field. With the three phase arrangement, as chosen for the **maxon**-EC-Motor, provisions were made for both Wye and Delta connections of the three winding segments. However, the Wye connection is preferred due to smaller currents permitting smaller cross sections of conductors and connections. Therefore, all further discussions will be based upon the Wye connection.

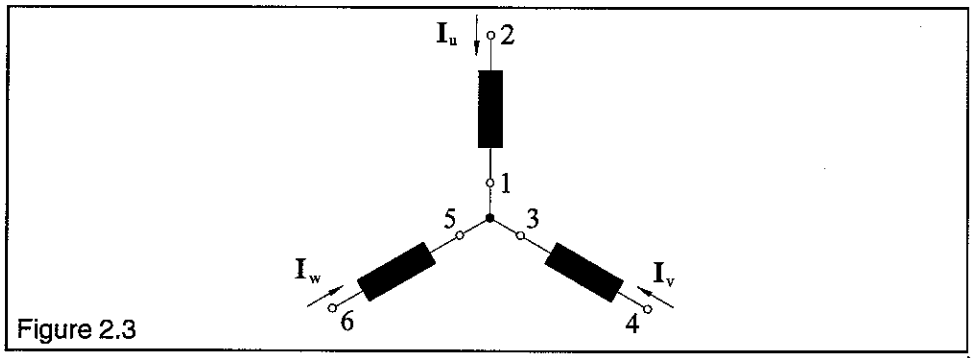

Figure 2.3

If we define the sense of the phase currents as shown, then the idealized current flow for two unique commutation systems can be represented graphically as follows.

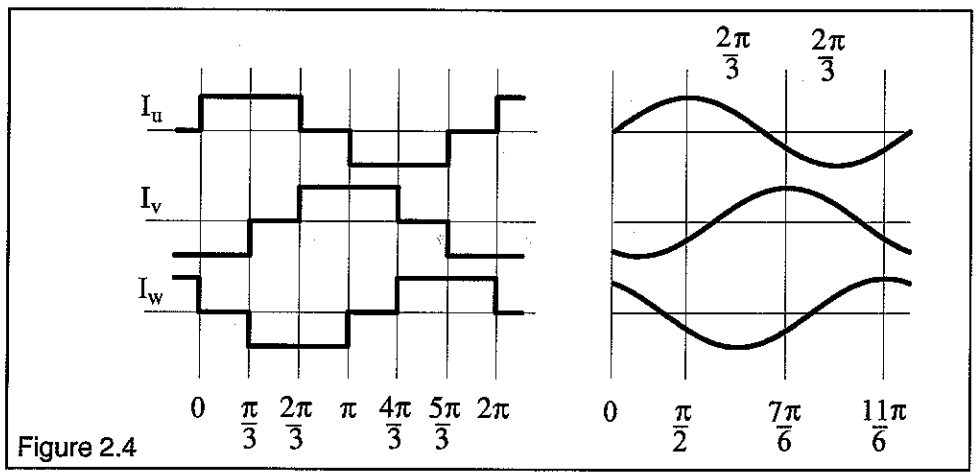

Figure 2.4

Both systems have unique requirements of the rotors angular position resolution with respect to the stator. The figure on the left constitutes the so called **Block commutation.** Here two winding segments are connected to a constant current supply, therefore a position resolution of $\pi/3 = 60°$ is sufficient to assure correct commutation. The figure on the right, so called **Sinusoidal commutation**, has all three winding segments connected to a sinusoidal current source simultaneously. Naturally a much finer resolution of rotor angular position is required to facilitate sinusoidal current flow.

A drawback of the simpler Block commutation lies in the fact that, as we shall see in the derivation of torque below, position dependant variations in torque occur during the constant current phase. On the other hand with the more cumbersome Sinusoidal commutation the generated torque can be held constant, at least theoretically, independent of rotor position. This control alternative is a requirement to assure much smoother operation of the EC-Motor throughout the entire rotational speed range, among other things.

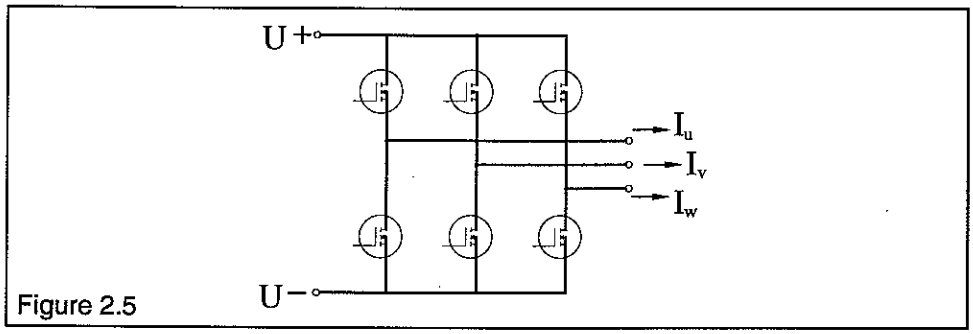

Figure 2.5

A possible choice for power electronics with either commutation system is shown in figure 2.5 as a simplified three phase bridge circuit utilizing power MOS-FETs.

## 2.5. Motor Characteristic Parameters

### 2.5.1. Torque

In order to calculate the forces acting on the rotor and the resulting torque we must first consider the current distribution in the winding. As we did for the bell rotor motor in section 1.7.1 we must determine which segments of the winding contribute to torque. We will assume that the motor has a two pole permanent magnet and has square wave current flow, refer to Figure 2.4, through the requisite winding segments.

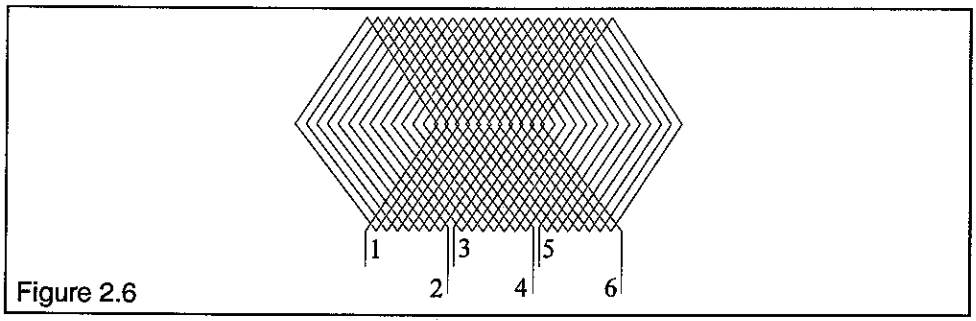

Figure 2.6

Figure 2.6 schematically represents a rhombic winding from a **maxon**-EC-Motor unwound in a plane with winding taps 1 through 6. Taps 1 and 2, 3 and 4 and 5 and 6 belong to the first, second and third winding segments respectively. The three winding segments are spatially separated by 120°, Wye connected and alternatingly connected to current I.

If we choose a stator field distribution as in 2.1 /f, then the current flow through the rhombic winding will be as in Figure 2.7. Current I flows into tap 2 and out of tap 1 of the first winding segment. Through the Wye connection the current flows into tap 3 and out of tap 4 of the second winding segment. The third win-

ding segment has no current flowing through it so it is not active in this phase and makes no contribution to torque.

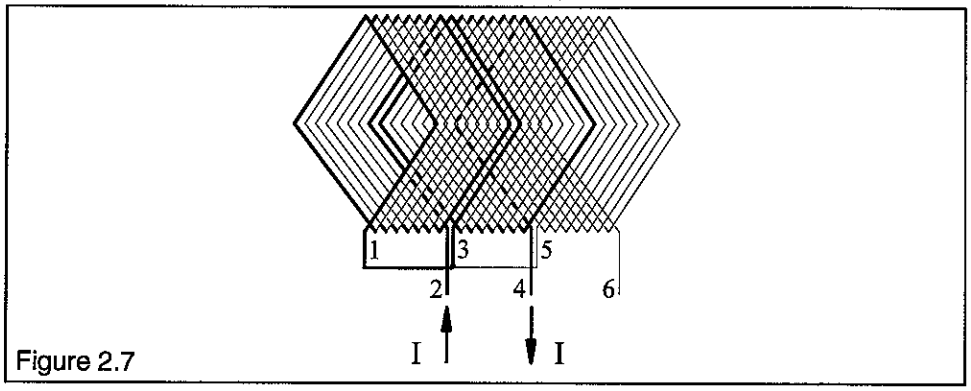

Figure 2.7

For better oversight we separate the two active winding segments between taps 2 and 3. If we look at the direction of current flow in the individual wires we can identify three distinct regions.

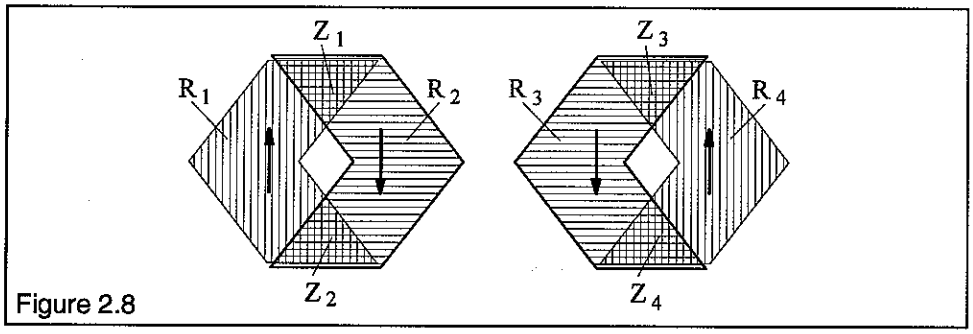

Figure 2.8

In the regions with heavy borders and horizontal hatching the current flows downwards, in the regions with light borders and vertical hatching the current flows upwards. The two inner rhombs without hatching have no current carrying conductors as the two active winding segments were pulled apart..
The triangles $Z_1$, $Z_2$, $Z_3$ and $Z_4$ have upwards and downwards flowing current overlapping, which cancels the forces due to the current, and make no contribution to torque.

If we reunite the two winding segments, by overlapping rhomb R2 with rhomb R3, we get resulting current surfaces as shown in Figure 2.9. Only regions contributing to the effective force are shown. Regions that are single effective get one arrow, regions that are double effective (overlapping) get two arrows.

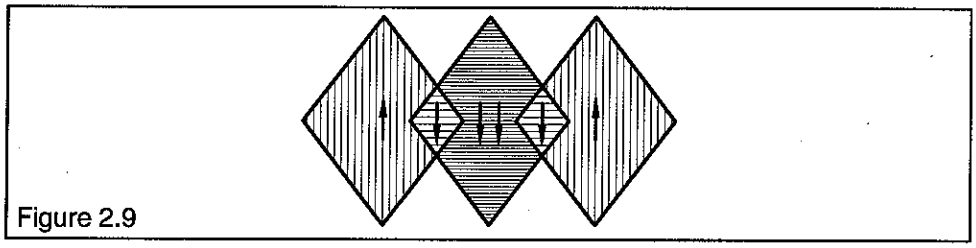
Figure 2.9

The current surfaces thus obtained are clearly oriented nevertheless not usable in their drawn form. However, using a trick we can get the overlapping rhombs

into the desired form. Simply separate the overlapping rhombs into same sized partial rhombs as shown below.

Figure 2.10

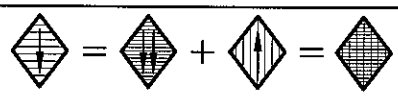

Thereby we get the current surfaces and rhombs into a form appropriate for our calculations.

Figure 2.11

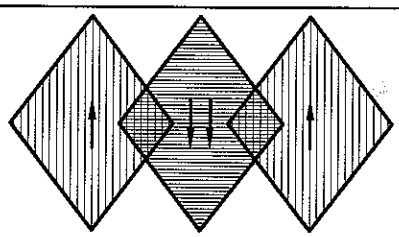

Now we can assign a single current surface to the complete rhomb 1, a double to rhomb 2 and a single to rhomb 4.

It can be shown that each of the six possible stator field variations can be similarly broken down into rhombs and current surfaces through this algorithm.

We will now determine the force resulting from each of the four rhombs and determine the net resulting force as a sum of the four force components $F_1$, $F_2$, $F_3$, $F_4$.

With the help of Eq. 1.25, we get the force dF, from a single current filament of length 2y within a single rhomb, as

Eq. 2.1 $dF = IB_o vr2y \sin\varphi d\varphi$

The relationship $y = a\varphi$ for length y of a current filament at location $\varphi$ is valid here to.

Now we divide rhomb 1 into a region I with $\varphi_o \le \varphi \le \varphi_o+\pi/2$ and a current filament of length $y = \ell/\pi\ (\varphi - \varphi_o)$ and a region II with $\varphi_o+\pi/2 \le \varphi \le \varphi_o+\pi$ and the respective current filament length $y = -\ell/\pi\ (\varphi - \varphi_o - \pi)$.

The following figure shows the relationships for rhomb 1

Figure 2.12

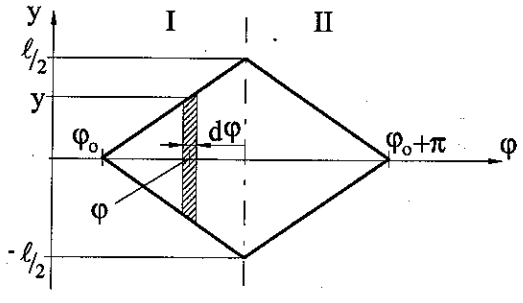

We can now start solving for force component $F_1$

Eq. 2.2

$$F_1 = 2IB_o v r \left( \int_{\varphi_o}^{\varphi_o+\pi/2} \frac{\ell}{\pi}(\varphi - \varphi_o)\sin\varphi\, d\varphi + \int_{\varphi_o+\pi/2}^{\varphi_o+\pi} -\frac{\ell}{\pi}(\varphi - \varphi_o - \pi)\sin\varphi d\varphi \right)$$

After integration, with consideration for the limits of integration, we get

Eq. 2.3 $$F_1 = \frac{4}{\pi} I B_o \ell v r \cos\varphi_o$$

We can work with rhombs 2 and 3 simultaneously; since they are congruent after removing the imaginary separation in the center of the winding. To make integration possible we again get a region I with $\varphi_O+2\pi/3 \le \varphi \le \varphi_O+7\pi/6$ and current filament length $y = \ell/\pi\ (\varphi - \varphi_O - 2\pi/3)$, as well as a region II with $\varphi_O+7\pi/6 \le \varphi \le \varphi_O+10\pi/6$ and current filament length $y = -\ell/\pi\ (\varphi - \varphi_O - 5\pi/3)$.

The following figure shows the relationships for rhomb 2 and 3

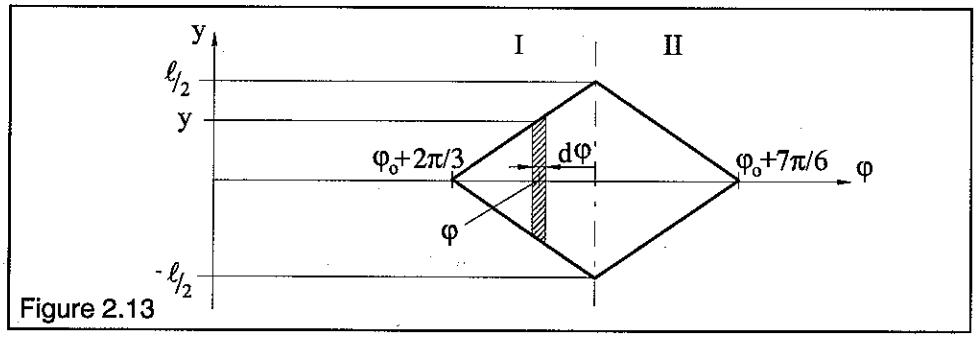

Figure 2.13

With this we can write for force components $F_2$ and $F_3$ (negative sign is required since current is flowing in the opposite direction through rhombs 2 and 3)

Eq. 2.4 $$F_2 = F_3 = -2IB_o v r \left( \int_{\varphi_o+4\pi/6}^{\varphi_o+7\pi/6} \frac{\ell}{\pi}(\varphi - \varphi_o - 2\pi/3)\sin\varphi\, d\varphi + \int_{\varphi_o+7\pi/6}^{\varphi_o+10\pi/6} -\frac{\ell}{\pi}(\varphi - \varphi_o - 5\pi/3)\sin\varphi d\varphi \right)$$

After integration, with consideration for the limits of integration, we get

Eq. 2.5 $$F_2 = F_3 = -\frac{4}{\pi} I B_o \ell v r \cos(\varphi_o + 2\pi/3)$$

Rhomb 4 connects directly to rhomb 3 and will be divided similarily for integration. So we get a region I $\varphi_O+4\pi/3 \le \varphi \le \varphi_O+11\pi/$ and current filament length $y = \ell/\pi\ (\varphi - \varphi_O - 4\pi/3)$ as well as region II with $\varphi_O+11\pi/6 \le \varphi \le \varphi_O+14\pi/6$ and current filament length $y = -\ell/\pi\ (\varphi - \varphi_O - 7\pi/3)$.

The following figure shows the relationships for rhomb 2 and 3

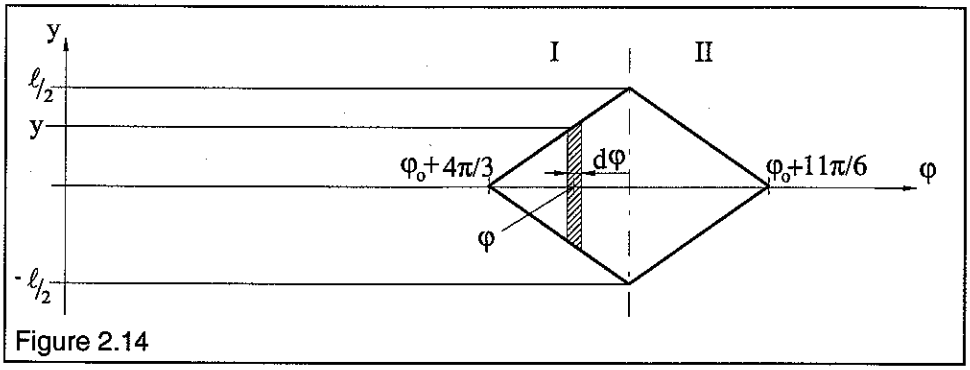

Figure 2.14

Eq. 2.6 $$F_4 = 2IB_o\nu r\left(\int_{\varphi_o+8\pi/6}^{\varphi_o+11\pi/6}\frac{\ell}{\pi}(\varphi-\varphi_o-4\pi/3)\sin\varphi\,d\varphi+\int_{\varphi_o+11\pi/6}^{\varphi_o+14\pi/6}-\frac{\ell}{\pi}(\varphi-\varphi_o-7\pi/3)\sin\varphi d\varphi\right)$$

After integration, with consideration for the limits of integration, we get

Eq. 2.7 $$F_4 = -\frac{4}{\pi}I\,B_o\ell\nu\,r\cos(\varphi_o+\pi/3)$$

With that we we can solve for the total force F as sum of the force components

Eq. 2.8 $$F = F_1+F_2+F_3+F_4 = \frac{2}{\pi}I\,B_o\ell\nu\,r\,f(\varphi_o)$$

We have combined the individual phase shifted trigonemetric functions of $\varphi_O$ into one for clarity

Eq. 2.9 $$f(\varphi_o) = 2\left[\cos\varphi_o-\cos(\varphi_o+\pi/3)-2\cos(\varphi_o+2\pi/3)\right]$$

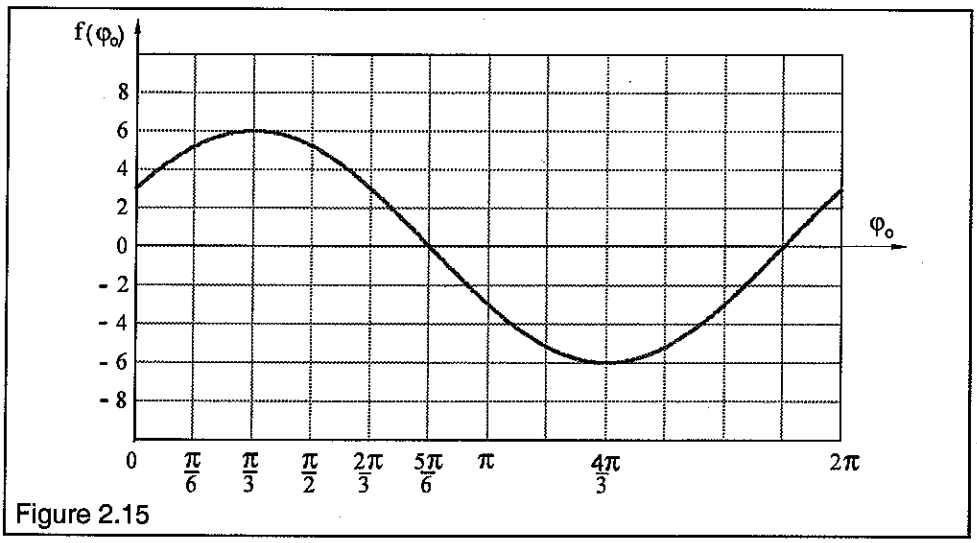

Figure 2.15

As the graph shows function $f(\varphi_O)$ has maxima and minima at $\varphi_O = \pi/3$ and $\varphi_O = 4\pi/3$. The , more interesting for us, maximum reaches the value of +6, while the minimum reaches the value -6.

Thereby we get the maximum value of the tangential force F as

Eq. 2.10 $$\hat{F} = \frac{12}{\pi} I B_o \ell v r$$

With the average radius r and the winding number w = 2πrv of the winding we get the maximum value for torque as

Eq. 2.11 $$\hat{M} = \frac{6}{\pi^2} I B_o r \ell w$$

The shape of $f(\varphi_O)$ according to Eq. 2.9 can, of course, be represented mathematically as an equivalent sinusoidal function. Thereby the generated torque $M(\varphi_O)$ becomes

Eq. 2.12 $$M = \hat{M} \sin(\varphi_o + \frac{\pi}{6})$$

This means that for our idealized Block commutation with three Wye connected winding segments : Even though we defined constant current, we get an angular position dependant torque for each of the six possible stator field distributions. If, as in figure 2.1, we label each of the six stator field distributions with the letters a,b,c,d,e,f, then shift the maximum torque by π/6 onto the next succesive stator field distribution, for each revolution of the rotor we get the following torque curve

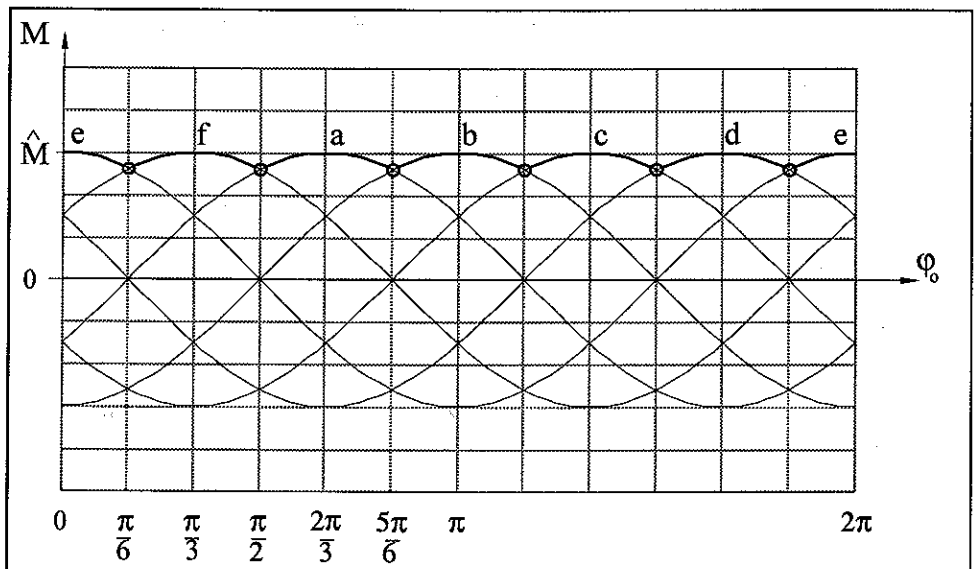

Figure 2.16

For these six stator field distributions we can calculate the average torque under any given set of operating cconditions. However this simplification is not possible for low angular speed or start up, see section 2.5.3.

For the performed mechanical work $W_{mech}$ of rotary motion the following is generally true, see also Eq. 1.76

Eq. 2.13 $$W_{mech} = \int_{\varphi_1}^{\varphi_2} M d\varphi = \overline{M} \Delta\varphi$$

For the relationships at hand, applied to a stator field distribution, we can write

Eq. 2.14 $$W_{mech} = \int_{\varphi_1}^{\varphi_2} M d\varphi_o = \int_{\pi/6}^{\pi/2} \hat{M} \sin(\varphi_o + \frac{\pi}{6}) d\varphi_o = \hat{M} \int_{\pi/6}^{\pi/2} \sin(\varphi_o + \frac{\pi}{6}) d\varphi_o = \overline{M} [\varphi_o]_{\pi/6}^{\pi/2}$$

Then for the average torque we get

Eq. 2.15 $$\overline{M} = \hat{M} \frac{3}{\pi} \int_{\pi/6}^{\pi/2} \sin(\varphi_o + \frac{\pi}{6}) d\varphi_o = 0.955 \hat{M} = 0.955 \frac{6}{\pi^2} I B_o r \ell w$$

or as current I(M)

Eq. 2.16 $$I = 1.047 \frac{\pi^2}{6} \frac{1}{B_o r \ell w} \overline{M}$$

Likewise we can give the torque constant

Eq. 2.17 $$\overline{k}_M = \frac{\overline{M}}{I} = 0.955 \frac{6}{\pi^2} B_o r \ell w$$

In the same manner as with the stator in the bell rotor motor the maximum value of air gap induction $B_O$ falls off slightly towards the ends of the magnet. We can compensate for this by modifying $B_O$ with an empirical factor $c_1 < 1$.

Routine like, we will study a slightly modified rhomb geometry. Specifically we would like to see if there are any advantages to partitioning the rhomb at 120° instead of 180°. We now get different current surfaces and 120° rhombs as shown below.

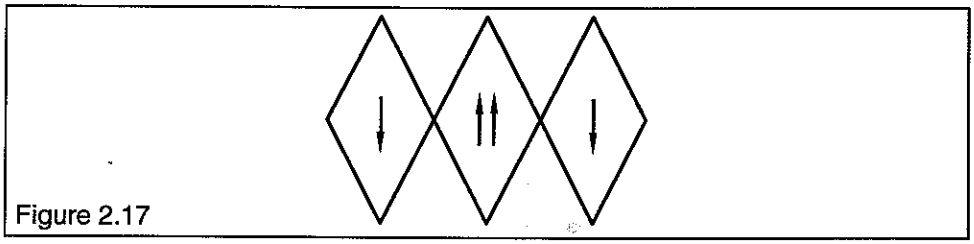

Figure 2.17

Following the same procedure as for the 180° rhombs with the only changes being rhomb slope and limits of integration.
We again define a region I with $\varphi_O \le \varphi \le \varphi_O + \pi/3$ and a current filament $y = \ell/\pi(\varphi - \varphi_O)3/2$ and a region II with $\varphi_O + \pi/3 \le \varphi \le \varphi_O + 2\pi/3$ and a current filament $y = -\ell/\pi(\varphi - \varphi_O - 2\pi/3)3/2$.

If we complete the calculations, then we get for the generated torque M

Eq. 2.18 $$M = \frac{1}{\pi^2} I B_o r \ell w g(\varphi_o)$$

We have combined the individual phase shifted trigonemetric functions of $\varphi_O$ into one for clarity as

Eq. 2.19 $g(\varphi_o) = \frac{3}{2}[\sin(\varphi_o + \pi/3) - \sin(\varphi_o + 2\pi/3) + 2\sin\varphi_o]$

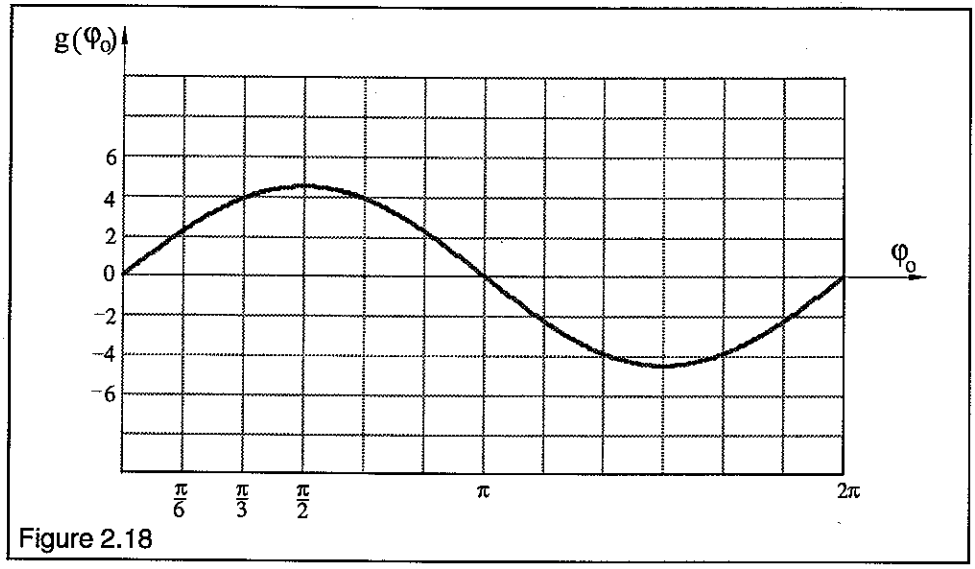

Figure 2.18

As the graph shows function $g(\varphi_O)$ has maxima and minima at $\varphi_O = \pi/2$ and $\varphi_O = 3\pi/2$. The, more interesting for us, maximum reaches the value of +4.5, while the minimum reaches the value -4.5.

Thereby we get the maximum value of the tangential force F for the 120° rhomb partition as

Eq. 2.20 $\hat{M} = \frac{4.5}{\pi^2} I B_o r \ell w$

with the ratio 4.5/6 = 0.75 the result is substantially less than the value of the 180° rhomb partition and will therefore not be pursued.

### 2.5.2. Rotational Speed

Reffering back to section 1.7.2 the rotational speed can be calculated as a function n(M) of torque. A simplified equivalent circuit of the Wye connected EC-Motor can be constructed as follows:

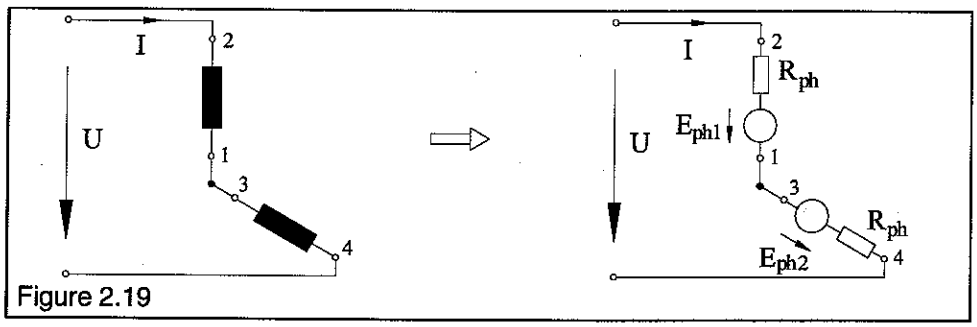

Figure 2.19

To generate a specific torque M, we need the current I determined by Eq. 2.16. If we use $R_{ph}$ to represent the impedance of a winding segment or phase then the following mesh equation is valid

Eq. 2.21 $U - E_{ph2} - E_{ph1} - 2IR_{ph} = 0$

The instantaneous values of voltage induced in the winding segments can be linked at any moment in time by

Eq. 2.22 $E_{ph} = E_{ph1} + E_{ph2}$

and if we calculate with a yet to be determined average value for induced voltage, we get for the sought current

Eq. 2.23 $$I = \frac{U - \overline{E}_{ph}}{2R_{ph}}$$

If we substitute Eq. 2.16 for current, then we get the relationship between generated torque and average induced voltage

Eq. 2.24 $$1.047 \frac{\pi^2}{6} \frac{1}{B_o r \ell w} \overline{M} = \frac{U - \overline{E}_{ph}}{2R_{ph}}$$

To determine rotational speed as a function of torque n(M) from here,we obviously need to determine the dependance of induced voltage on rotational speed E(n) next.
For the calculations we will assume 180° rhombs and therefore we can utilize the calculations from section 1.7.2 for Eq. 1.55. Thereby we get for the induced voltage in a linear element ds of a winding segment

Eq. 2.25 $$dE_{ph} = \frac{4}{\pi} B_o \ell r^2 \nu \omega \sin \varphi_o d\varphi_o$$

Conditional upon the geometric arrangement of the winding segments the following dependance of the induced voltage $E_{ph}$ on the angle $\varphi_o$ results

Eq. 2.26 $$E_{ph} = \frac{4}{\pi} B_o \ell r^2 \nu \omega \left( \int_{\varphi_o}^{\varphi_o + 2\pi/3} \sin \varphi_o d\varphi_o + \int_{\varphi_o + 2\pi/3}^{\varphi_o + 4\pi/3} \sin \varphi_o d\varphi_o \right)$$

In order to fix the optimum alignment of the conducting phases we must determine the maximum of this function and get with $\varphi_o = \pi/3$

Eq. 2.27 $$\hat{E}_{ph} = \frac{12}{\pi} B_o \ell r^2 \nu \omega$$

The instantaneous induced voltage $E_{ph}$ in the winding segments varies sinusoidally at constant rotational speed and can be represented as

Eq. 2.28 $$E_{ph} = \hat{E}_{ph} \sin \omega t$$

As with the torque calculation, here to we must calculate with the average value during a conducting phase. If we assume that each of the six conducting phases covers an angle of $\pi/3$ and is symetric about the maximum value, then the average induced voltage within a conducting phase can be determined as follows

Eq. 2.29 $$\overline{E}_{ph} = \frac{3}{\pi}\int_{\pi/3}^{2\pi/3} \hat{E}_{ph} \sin \omega t d\omega t = \frac{3}{\pi}\hat{E}_{ph} = 0.995\hat{E}_{ph}$$

and further with $\omega = 2\pi n$ as well as $v = w/2r\pi$

Eq. 2.30 $$\overline{E}_{ph} = 0.955\frac{12}{\pi} B_o \ell r w n$$

If we substitute this result into Eq. 2.24, we get the sought after relationship between torque and rotational speed

Eq. 2.31 $$n = \frac{1}{0.955}\frac{\pi}{12}\frac{U}{B_o \ell r w} - 1.047\frac{\pi^3}{36}\frac{R_{ph}}{(B_o \ell r w)^2}\overline{M}$$

We obtained an analgous dependance for the bell rotor motor with Eq. 1.59. If we call upon the torque constant $k_M$ from Eq. 2.17 again, then we get

Eq. 2.32 $$n = \frac{1}{2\pi}\left(\frac{U}{\overline{k}_M} - \frac{2R_{ph}}{\overline{k}_M^2}\overline{M}\right)$$

With this linear equation we can determine the intercepts in the coordinate system n(M).
For the case M = 0, this defines a motor operating with no load and no loss torque $M_V$, we get the so called ideal no load speed $n_i$

Eq. 2.33 $$n_i = \frac{1}{2\pi}\frac{U}{\overline{k}_M}$$

and with n = 0, defining a motor with locked rotor, the so called ideal stall torque

Eq. 2.34 $$\overline{M}_{iH} = \frac{U}{2R_{ph}}\overline{k}_M$$

A further characterizing parameter is the so called stall current $I_H$

Eq. 2.35 $$I_H = \frac{U}{2R_{ph}}$$

Conditional upon the position dependant torque in each of the six stator field distributions, the actual stall torque can be further reduced. Mathematically the ideal stall torque, depending upon rotor position, is in the range of

Eq. 2.36 $$M_{iH\,min} = 0.866\frac{\hat{M}}{I}I_H \le \overline{M}_{iH} \le \frac{\hat{M}}{I}I_H$$

where the torque determined by Eq. 2.11 is to be substituted in for the maximum value.

In reality the ideal no load speed $n_i$ as well as ideal stall torque $M_{iH}$ can not be realized. In both cases the loss torque $M_V$ will cause a corresponding reduction.
With this we can represent the dependance of torque M on rotational speed n at constant voltage U graphically

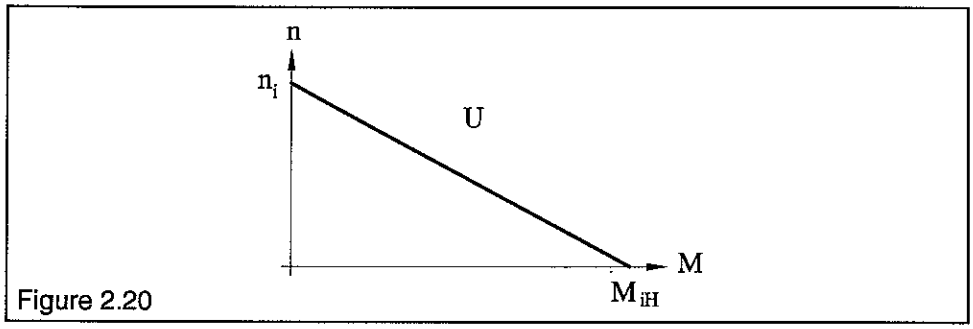

Figure 2.20

With the two parameters $n_i$ and $M_{iH}$ we can define the average speed/torque gradient $\Delta n/\Delta M$ as

Eq. 2.37 $$\frac{\Delta n}{\Delta M} = \frac{n_i}{M_{iH}} = \frac{1}{2\pi}\frac{2R_{ph}}{\bar{k}_M^2}$$

Thereby we can rewrite Eq. 2.32 as

Eq. 2.38 $$n = n_i\left(1 - \frac{M}{M_{iH}}\right) = n_i - \frac{\Delta n}{\Delta M}M$$

If we set $M = M_{Vo}$, that is the only active load is loss torque, we get the effective no load speed $n_o$ as

Eq. 2.39 $$n_o = n_i - \frac{\Delta n}{\Delta M}M_{Vo}$$

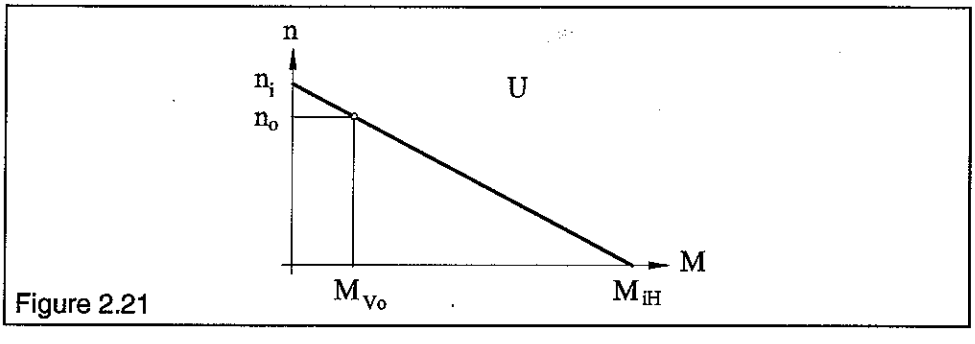

Figure 2.21

Thereby we get the same basic graphic representation as for the bell rotor motor. The change to the speed/torque gradient due to winding temperature rise follows the same rules as shown in Figure 1.34.

We will now compare the speed/torque gradient of an bell rotor motor with an EC-motor of the same active part's geometric size. The dimensions of the per-

manent magnet, air gap and winding should be equivalent. Thereby the calculations will be performed with equal $B_O$, $\ell$, r and total winding turn count.
For the bell rotor the winding resistance is determined by the parallel connection of the two winding halves simplified as

Eq. 2.40 $$R_{Rot} = \frac{1}{4} R$$

where R represents the resistance of all series connected windings.
The torque constant for the bell rotor is given by

$$k_{MGl} = \frac{4}{\pi^2} B_o r \ell w$$

For the Wye connected EC-Motor the resistance for the two series connected phases is

Eq. 2.41 $$2R_{ph} = \frac{2}{3} R$$

and the average torque constant of the EC-Motor is given by

$$\overline{k}_M = 0.955 \frac{6}{\pi^2} B_o r \ell w$$

The relationship between speed/torque gradients of an EC-motor and bell rotor motor is

Eq. 2.42 $$\frac{\Delta n / \Delta M|_{EC}}{\Delta n / \Delta M|_{Gl}} = \frac{\frac{2}{3} R}{\frac{1}{4} R} \frac{\pi^4}{0.955^2 36} \frac{16}{\pi^4} = 1.299$$

The speed/torque gradient of the Wye connected, Block commutated EC-motor is approximately 30% steeper than an equivalent bell rotor motor. This is mainly due to the fact that the EC-motor has much lower winding utilization, as only 2/3 of all winding turns are actively contributing to torque at any given time. Furthermore the torque variation reduces the average torque value used in the calculation.

### 2.5.3. Starting Process and Oscillation Characteristics

The equation of motion for a rotating system given in section 1.7.3 is valid for an EC-motor as well. However the rotor's moment of inertia $J_R$ is greater than for a comparable bell rotor motor.

$$M_B = J_R \frac{d\omega}{dt} = 2\pi J_R \frac{dn}{dt}$$

According to Eq. 1.73 the mechanical time constant $\tau_{mges}$ for a coupled system is

$$\tau_{mges} = (J_R + J_b)2\pi \frac{n_i}{M_{iH}}$$

For no load acceleration the rotational speed n increases approximately exponentially until it reaches the no load speed $n_o$, see Eq. 1.72. The disproportionate increase in iron losses with increase in rotational speed cause the acceleration curve to flatten in the upper speed ranges.

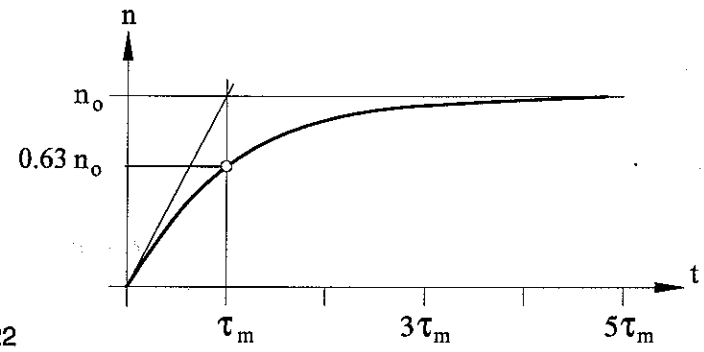

Figure 2.22

The statorfield's torque acting upon the rotor and the total moment of inertia of the rotor (rotor inertia and load inertia) form a system apt to oscillate. Therefore we will approximate the natural frequency, specifically the period of vibration $T_R$, of the rotor.

For free torsional vibration there is a general interdependence between the period of vibration $T_R$, moment of inertia $J = J_R + J_b$ and resetting torsion torque $M_T$

Eq. 2.43 $$T_R = 2\pi\sqrt{\frac{J}{M_T}}$$

Normally the assumption that resetting torsion torque is proportional to the angular excursion ($M_T = c_T\varphi_O$) is valid. However in the case at hand, the torque, according to the function $f(\varphi_O)$, is by no means proportional to the angle of rotation. The approximation can still be solved with satisfactory accuracy through linearization in the critical switching zone. We will therefore substitute in the effective slope of the torque curve at the switching point for resetting torsion torque.

Eq. 2.44
$$M_T = \left.\frac{dM}{d\varphi_o}\right|_{\pi/6} = \hat{M}\frac{d\sin(\varphi_o + \pi/6)}{d\varphi_o} = \hat{M}\cos(\varphi_o + \pi/6)\Big|_{\pi/6} = 0.5\hat{M}$$

If oscillations outside of the linearized range need to be considered, for the period of vibration formally the equals sign must be replace with a ≥. Thereby we get for the free, undamped period of vibration $T_R$ of the rotor

Eq. 2.45 $$T_R \geq 2\pi\sqrt{\frac{J}{0.5\hat{M}}}$$

As long as the period of vibration $T_R$ is large by comparison to time $\Delta t$ between two successive switches of the stator field

Eq. 2.46 $$2\pi\sqrt{\frac{J}{0.5\hat{M}}} >> \Delta t = \frac{1}{6}n$$

the system cannot follow the torque variation in a single phase and an average torque acts upon the rotor, as previously derived in Eq. 2.15.

Eq. 2.47 $$\overline{M} = 0.955\frac{6}{\pi^2} I B_o r \ell w$$

If $T_R >> \Delta t$ is not met, mild to severe flutter, especially at low speeds, becomes apparent. By increasing the moment of inertia this property can be improved, however an increase in the mechanical time constant $\tau_{mech}$ must also be dealt with.

### 2.5.4. Power

As shown in section 1.7.4, the following holds for motor power output

$$P_{mech} = M_b \omega = M_b 2\pi n$$

The generated torque M is divided amongst output torque $M_b$ and loss torque $M_V$, therefore $M = M_b + M_V$ is valid. A simplified start to determining the loss torque $M_V$ by assuming it as a constant, independent of rotational speed n, is not plausible for an EC-motor.
As we will see in section 2.5.6, in addition to frictional losses there will be iron losses $P_{Fe}$ that increase exponentially with rotational speed.
We include this complication in the calculation of loss torque $M_V$ by adding a term dependant on rotational speed to the constant portion (a linear increase of loss torque carries through as a squared increase to power loss).

Eq. 2.48 $$M_V = M_{VA} + c_5 n$$

The relationship of rotational speed n and torque M can be presented as

Eq. 2.49 $$n = n_i - \frac{\Delta n}{\Delta M} M = n_i - \frac{\Delta n}{\Delta M}(M_b + M_{VA} + c_5 n)$$

We can solve for the relationship of rotational speed n and load torque $M_b$ as

Eq. 2.50 $$n = \frac{n_i - \frac{\Delta n}{\Delta M}(M_b + M_{VA})}{1 + \frac{\Delta n}{\Delta M} c_5}$$

If we substitute this into the equation for mechanical power output $\Delta n/\Delta M = n_i/M_{iH}$, we get

Eq. 2.51 $$P = P_{mech} = M_b 2\pi n = 2\pi \frac{n_i M_b - \frac{n_i}{M_{iH}}(M_b^2 + M_{VA} M_b)}{1 + \frac{n_i}{M_{iH}} c_5}$$

The maximum of this function and thereby the torque $M_P$ at maximum power is determined by setting the first derivative equal to zero

Eq. 2.52 $$M_P = \frac{M_{iH} - M_{VA}}{2}$$

Substituting into the power equation yields the maximum power $P_{max}$ as

Eq. 2.53 $$P_{max} = \frac{\pi}{2} n_i \frac{(M_{iH} - M_{VA})^2}{M_{iH} + n_i c_5}$$

If we compare this result to the result of Eq. 1.83,for the bell rotor motor, we find that, due to the iron losses, the maximum power output $P_{max}$ is slightly smaller.

For the graphic representation the rotational speed dependant loss torque $M_V$ is purposefully exaggerated.

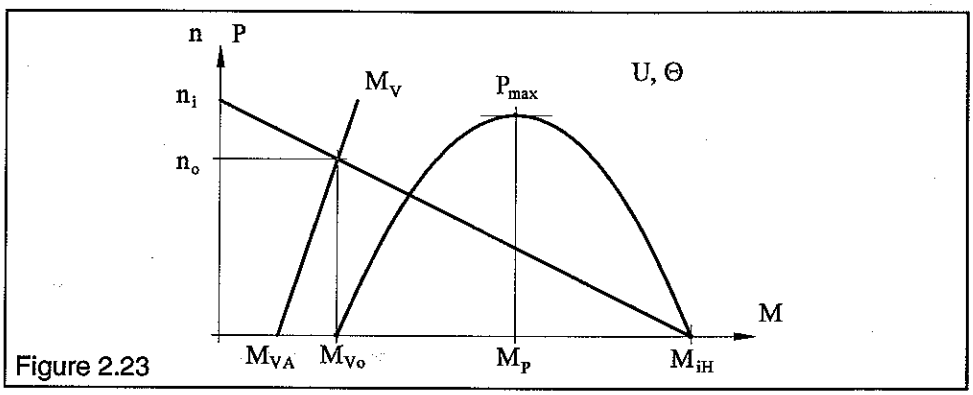


Figure 2.23

In actual applications the EC-motor can only be operated at maximum power $P_{max}$ if the load torque $M_b$ does not exceed the limit $M_b \leq M_{zul} = k_M I_{zul}$.

## 2.5.5. Efficiency

We use the definition of efficiency from Eq. 1.84

$$\eta = \frac{P}{P_{zu}}$$

As previously discussed in section 2.5.4, we will use a rotational speed dependant increase to the loss torque $M_V = M_{VA} + c_5 n$ so we at least include an approximation of the iron losses. For power output P we can use Eq. 2.51 directly.

$$P = P_{mech} = M_b 2\pi n = 2\pi \frac{n_i M_b - \frac{n_i}{M_{iH}}(M_b^2 + M_{VA} M_b)}{1 + \frac{n_i}{M_{iH}} c_5}$$

With power input $P_{zu}$, Eq. 2.33 and Eq. 2.16 for $n_i$ and I the efficiency is expressed in the following form

Eq. 2.54 $$\eta = \frac{(M_{iH} - M_{VA})M_b - M_b^2}{(M_b + M_{VA} + c_5 n_i)M_{iH}}$$

Comparing this to the efficiency of the bell rotor motor, the additional term $c_5 n_i$ in the denominator reduces the efficiency $\eta$. we can see the general shape of the efficiency curve in Figure 1.37. The figure shows a comparison to an equivalent bell rotor motor. The torque/speed gradient factors $n_i$ and $M_{iH}$ were kept equivalent for the calculations.

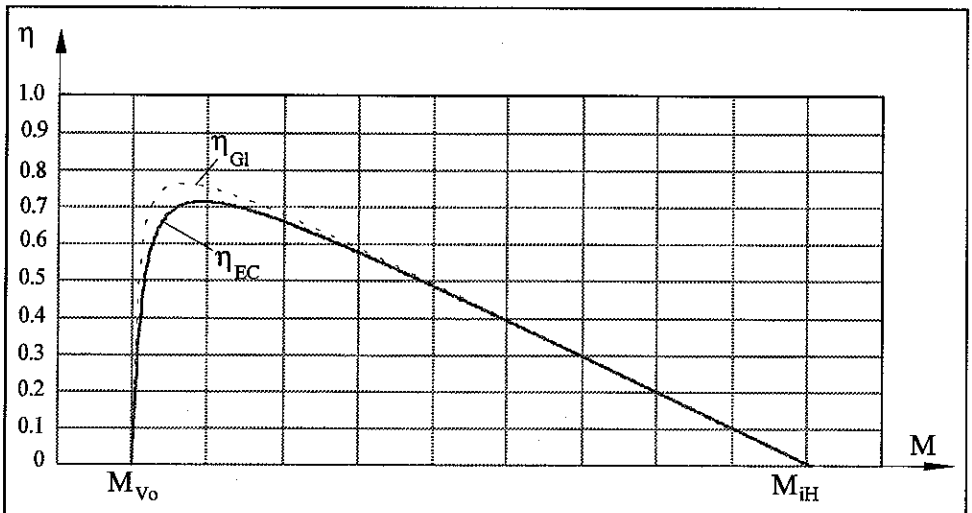


Figure 2.24

Therefore the efficiency of an EC-motor is slightly lower than for the bell rotor motor throughout the operating range.
We can solve for the maximum value of the efficiency function by setting the first derivative equal to zero.

$$\frac{d\eta}{dM_b} = 0$$

With several simplifications we get the maximum efficiency relationship

Eq. 2.55 $$\eta_{max} \approx \left(1 - \sqrt{\frac{M_{VA} + c_5 n_i}{M_{iH}}}\right)^2 = \left(1 - \sqrt{\frac{I_o}{I_H}}\right)^2$$

As we see here again, the maximum efficiency value is slightly lower when compared to Eq. 1.92 for the bell rotor motor.

### 2.5.6. Iron Losses

The stator, serving as magnetic return path, has a rotating magnetic field impressed upon it by the rotating permanent magnet. Due to this, two independent sources for iron losses result.

Eq. 2.56 $$P_{Fe} = P_{FeH} + P_{FeW}$$

We will now study the determining characteristic values for the development of these losses in detail.

### 2.5.6.1. Hysteresis Losses

The sheet metal used in the magnetic flux directing stator is characterized by its hysteresis cycle. During each magnetization reversal process, caused by the permanent magnet's rotation, the energy defined by the surface of the hysteresis loop is converted into heat.
To approximate these magnetization reversal or hysteresis losses $P_{FeH}$ we are dependant on empirical relationships. For homogeneous, sinusoidally varying magnetization reversals in hot rolled steel sheet the losses can be defined as follows:

Eq. 2.57 $$P_{FeH} \approx c_H n B^{1.6}$$

For cold rolled sheet additional effects due to material anisotropy occur (the materials magnetic characteristics are not equivalent in rolled and perpendicular to rolled directions).
For an EC-motor the hysteresis losses $P_{FeH}$ in the stator principally increase linearly with rotational speed. The linear relationship of the hysteresis losses $P_{FeH}$ to rotational speed n and the exponential relationship of induction amplitude $B_0$ is determined exclusively by the quality of the steel used (material constant $c_H$ ). The actual occurring value of induction amplitude $B_0$ is determined by the sizing of the magnetic circuit.

### 2.5.6.2. Eddy Current Losses

The rotating magnetic field of the rotor generates eddy currents in the surrounding stator steel due to its conductivity. These eddy currents cause additional losses. To minimize the eddy current losses the stator is not constructed of a single ingot. Instead, a stack of electrically insulated sheet metal rings (laminations) makes up the return path (stator stack).
We will now examine the pertinent conditions in a segment of a lamination and learn the factors influencing the resulting power loss.

In a metallic conductor the physical relationship between current density S and electric field intensity E is given by conductivity k. The subscript W shall identify an association with eddy currents.

Eq. 2.58 $$S_W = \kappa E_W$$

The current is defined independently as current density times corresponding surface area

Eq. 2.59 $$dI_W = S_W dA$$

If we define the current as electric charge per unit time we get

Eq. 2.60 $$dQ_W = dI_W dt = S_W dA\, dt$$

With the voltage $U_W$ as a linear integral of field intensity $E_W$ along ds

Eq. 2.61 $$U_W = \int_s E_W ds \qquad dU_W = E_W ds$$

yields for energy $dW_W$ as a product of charge and voltage

Eq. 2.62 $$dW_W = dQ_W dU_W$$

Eq. 2.63 $dW_W = S_W dA\, dt\, E_W ds = S_W E_W dA\, ds\, dt = S_W E_W dV dt$

Thereby the power density per unit volume $dP_W$

Eq. 2.64 $$dP_W = \frac{dW_W}{dt\, dV} = S_W E_W$$

and for power $P_W$ integrated over the entire volume

Eq. 2.65 $$P_W = \int_V dP_W dV = \int_V S_W E_W dV = \kappa \int_V E_W^2 dV$$

In order to determine the dependance of field intensity on induction E(B) we will again call upon the law of induction

Eq. 2.66 $$U_W = -\frac{d\Phi}{dt} = -\frac{d}{dt}\int_A \mathbf{B} \cdot d\mathbf{A} = \oint_s \mathbf{E}_W \cdot d\mathbf{s}$$

Lets study a lamenation element under these conditions more closely. Relating the dimensions to an EC-motor's internal geometry, D is along the lamenation's axial thickness, b is radial and a is circumferential along the stator bore.

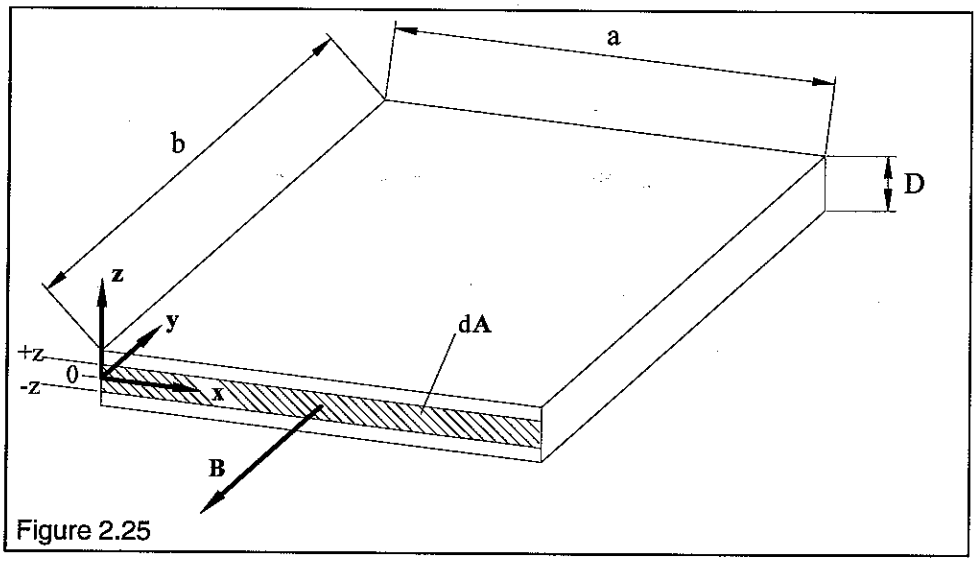

Figure 2.25

If we perform the integration referencing figure 2.25 we get

Eq. 2.67 $$-\frac{d}{dt}\int_A BdA = -\frac{dB}{dt}\int_0^a \int_{-z}^{+z} dxdz = -\frac{dB}{dt} a2z$$

Eq. 2.68 $$\oint E_w ds = E_W\left(2\int_0^a dx + 2\int_{-z}^{+z} dz\right) = E_W(2a + 4z)$$

Since z << a the term 4z can be neglected, this simplification yields

Eq. 2.69 $\oint E_w ds \cong E_W 2a$

Thereby we get the sought relationship with Eq. 2.65 and Eq. 2.67

Eq. 2.70 $E_W = -\frac{dB}{dt} z$

substituted into Eq. 2.65 for power $P_W$

Eq. 2.71 $$P_W = \kappa \int_V E_W^2 dV = \kappa \int_0^a \int_0^b \int_{-D/2}^{+D/2} E_W^2 dx dy dz = \kappa a b \left(\frac{dB}{dt}\right)^2 \int_{-D/2}^{+D/2} z^2 dz =$$

$$= \kappa a b \frac{D^3}{12} \left(\frac{dB}{dt}\right)^2$$

If we relate power $P_W$ to volume V = a b D, we get for power density $P_{WV}$

Eq. 2.72 $\frac{P_W}{V} = P_{WV} = \frac{1}{12} \kappa D^2 \left(\frac{dB}{dt}\right)^2$

We will assume that the induction, throughout the lamination's cross section, is not appreciably reduced by the eddy currents and varies cyclically with the angular velocity of the rotating permanent magnet. Then we can represent the temporal dependance of B with $B = B_o \sin\omega t$. Substituting into Eq. 2.72 we get for power density $P_{WV}$

Eq. 2.73 $P_{WV} = \frac{1}{12} \kappa D^2 \omega^2 B_o^2 \cos^2 \omega t$

The function $\cos^2\omega t$ is cyclical with a period $\pi$. Thereby we can determine the arithmatic (temporal) average of power density as follows

Eq. 2.74 $\overline{P}_{WV} = \frac{1}{12} \kappa D^2 \omega^2 B_o^2 \frac{1}{\pi} \int_0^\pi \cos^2 \omega t \, d(\omega t)$

Eq. 2.75 $\frac{1}{\pi} \int_0^\pi \cos^2 \omega t \, d(\omega t) = \frac{1}{\pi} \left[\frac{1}{4} \sin 2x + \frac{1}{2} x\right]_0^\pi = \frac{1}{2}$

With $\omega = 2\pi n$ we get

Eq. 2.76 $\overline{P}_{WV} = \frac{1}{24} \kappa D^2 \omega^2 B_o^2 = \frac{\pi^2}{6} \kappa D^2 n^2 B_o^2$

If we utilize the relationship of conductivity $\kappa$ with resistivity $\rho$ as $\kappa = 1/\rho$, we get

Eq. 2.77 $\overline{P}_{WV} = \frac{\pi^2}{6} \frac{D^2 n^2 B_o^2}{\rho}$

If we introduce the density $\gamma$, we get for mean eddy current losses in terms of mass

Eq. 2.78 $$\overline{P}_{Wm} = \frac{\pi^2}{6} \frac{D^2 n^2 B_o^2}{\gamma \rho}$$

Therefore, for an EC-motor the eddy current losses $P_{FeW}$ increase with the square of rotational speed n, lamination thickness D and induction $B_o$. The density $\gamma$ as well as the resistivity $\rho$ of the lamination affect eddy current losses linearly.

Now let us introduce another effect, besides power dissipation $P_{FeW}$, of the eddy currents The appearance of eddy currents $I_W$ generates a magnetic field $H_W$ and magnetic induction $B_W$ which serves to reduce the effective induction in the stator.

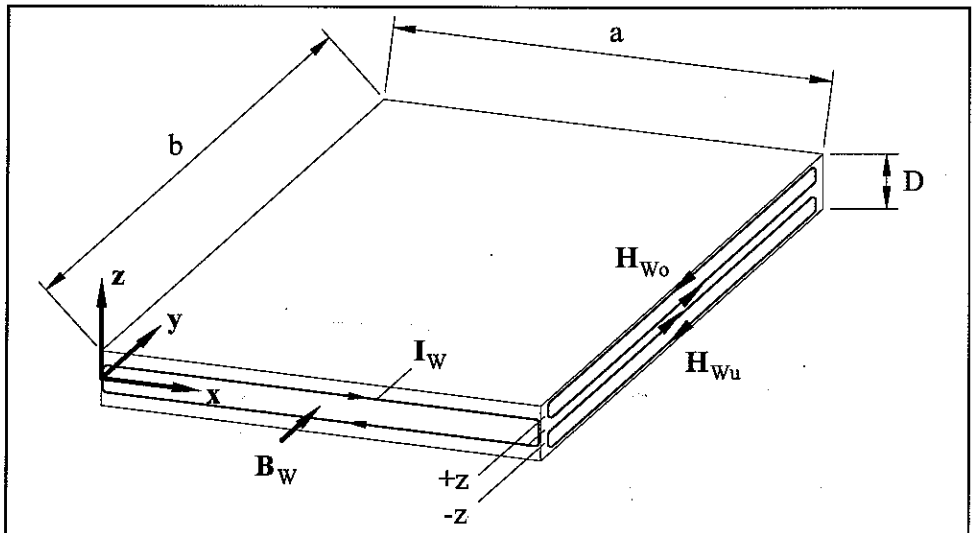

Figure 2.26

To estimate the generated magnetic field $H_W$ we will look back at the previous calculation of the eddy current losses. With Eq. 2.58 for current density $S_W$ we get for the current $I_W$ flowing through the flat element dA = b dz

Eq. 2.79 $$dI_W = \kappa E_W b\, dz$$

which flows more or less parallel to the x axis. We can calculate the current for the lamenation's upper half by integrating half of the lamination thickness D/2 with help from Eq. 2.70.

Eq. 2.80 $$I_W = \kappa b \int_0^{D/2} E_W dz = \kappa b \frac{dB}{dt} \int_0^{D/2} z dz = \frac{1}{8} \kappa b D^2 \frac{dB}{dt}$$

We get an equal value, opposite sense current in the lower lamination half. With help from the magnetic flux theorem we get current $I_W$ in terms of magnetic field $H_W$.

Eq. 2.81 $$\oint_s H_{Wo}\,ds = I_W = H_{Wo}\,2\left(\int_0^b dy + \int_0^z dz\right) = H_{Wo}(2b+2z)$$

Since z << b we can drop the term 2z, this simplification yields

Eq. 2.82 $$H_{Wo} = \frac{I_W}{2b} = H_{Wu}$$

In the lamination's center where z = 0 the two fields are additive and we get the complete magnetic field $H_W$ generated by the eddy current $I_W$.

Eq. 2.83 $$H_W = \frac{1}{8}\kappa D^2 \frac{dB}{dt}$$

If we take the time dependance of the induction on the angular velocity of the rotating permanent magnet $B = B_0 \sin \omega t$ into account, we get

Eq. 2.84 $$H_W = \frac{1}{8}\kappa D^2 \omega B_o \cos \omega t$$

For the amplitude of the magnetic field $H_W$ with $\omega = 2\pi n$ and $\kappa = 1/\rho$ we get

Eq. 2.85 $$\hat{H}_W = \frac{1}{8}\kappa D^2 \omega B_o = \frac{\pi}{4}\frac{D^2 n B_o}{\rho}$$

In the stator pack the known relationship between Magnetic field strength H and induction B is defined by the permeability $\mu$.

Eq. 2.86 $$B = \mu_r \mu_o H$$

So that the influence of the eddy current can be neglected the following must be true for the induction amplitude

Eq. 2.87 $$\hat{B}_W = \mu_{ra}\,\mu_o\,\hat{H}_W << B_o$$

Since we must be a safe distance from the saturation induction, we can substitute the starting permeability of the stator stack without introducing a large error.
This yields with Eq. 2.85 a limit on maximum permissible rotational speed n

Eq. 2.88 $$n << \frac{4}{\pi}\frac{\rho}{D^2 \mu_{ra}\,\mu_o}$$

### 2.5.7. Thermal Characteristics

The losses $P_V$ generated in an EC-motor have three main contributing causes. The relative contribution of each depends upon operating conditions. The rotational speed dependant iron losses $P_{Fe}$ are in addition to frictional losses $P_R = M_V\omega$ and Joule's losses $P_J = I^2 R_{W\Theta}$. See sections 2.5.6.1 and 2.5.6.2

Eq. 2.89 $$P_V = P_R + P_J + P_{Fe} = M_V\omega + I^2 R_{W\Theta} + P_{Fe}(n)$$

Comparing to the bell rotor motor, brush friction is no longer a factor but this is more than compensated for, especially at high rotational speed, by the iron los-

ses. Therefore the extremely high maximum efficiency of the bell rotor motor cannot be attained by the EC-motor.

### 2.5.7.1. Maximum Power Dissipation

The derivation in section 1.7.7.1 and accompanying analogous electric circuit for heat transfer are fully applicable to the EC-motor. Replacing the maximum permissible rotor temperature $\Theta_{Rmax}$ is the maximum permissible winding temperature$\Theta_{Wmax}$. The internal thermal resistance $R_{th1}$ is smaller than for the bell rotor motor which is directly attributable to the better thermal conductivity between winding and stator housing. We get then, with help from Eq. 1.98

Eq. 2.90 $$P_{Vzul} = \frac{\Theta_{W\,max} - \Theta_U}{R_{th1} + R_{th2}}$$

and the appropriate gauging temperatures of stator housing and winding

Eq. 2.91 $$\Theta_G = \Theta_U + P_V R_{th2}$$

Eq. 2.92 $$\Theta_W = \Theta_U + P_V (R_{th1} + R_{th2})$$

The accompanying analogous electric circuit for heat transfer can be derived from Figure 1.40.

### 2.5.7.2. Maximum Load Current

It is regrettably not possible to perform an accurate derivation of maximum permissible load current $I_{zul}$ for the entire operating range because the rotational speed dependant iron losses $P_{Fe}$ can only be determined empirically. Therefore we will restrict our derivation to the lower rotational speed range (n < 5000 $min^{-1}$), and neglect iron and frictional losses $P_{Fe}+P_R$, the only losses we will consider are Joule's losses $P_J$.
Assuming Wye connected Block commutation (see figure 2.3), at any moment in time only two of the three winding segments are conducting. The generated Joule's losses are however distributed throughout all three winding segments by cyclic switching of the segments.
If we represent the winding segments resistance $R_{Ph\Theta}$ at temperature $\Theta$ we can write

Eq. 2.93 $$P_{Vzul} = P_J = I_{zul}^2 2R_{Ph\Theta max}$$

With the resistance dependance on temperature we get, similarly to Eq. 1.104

Eq. 2.94 $R_{Ph\Theta} = R_{Ph25}[1 + \alpha_{Cu}(\Theta - 25)]$ specifically
$R_{Ph\Theta max} = R_{Ph25}[1 + \alpha_{Cu}(\Theta_{W\,max} - 25)]$

From these equations we get the maximum permissible effective current $I_{zul}$ as

Eq. 2.95 $$I_{zul} = \sqrt{\frac{P_{Vzul}}{2\,R_{Ph\Theta max}}}$$

or including thermal resistance and temperature

Eq. 2.96 $$I_{zul} = \sqrt{\frac{\Theta_{W\,max} - \Theta_U}{2\,R_{Ph\Theta max}(R_{th1} + R_{th2})}}$$

As can be deduced, the effect of increasing the maximum permissible winding temperature $\Theta_{Wmax}$ is greater on the maximum permissible load current $I_{zul}$ than is lost through the requisite increases in winding resistance $R_{ph\Theta max}$.

### 2.5.7.3. Warming and Thermal Time Constants

The derivation in section 1.7.7.3 is fully applicable to the **maxon**-EC-motor. Replacing rotor temperature and stator temperature is winding temperature and housing temperature respectively. Analogous to Eq. 1.114 we define a thermal time constant $\tau_{th1}$

Eq. 2.97 $$\tau_{th1} = R_{th1} C_W = R_{th1} m_W c_W$$

Analogous to Eq. 1.118 we get the following relationship for winding temperature $\Theta_W$

Eq. 2.98 $$\Theta_W = \Theta_G + P_V R_{th1}\left(1 - e^{-\frac{t}{\tau_{th1}}}\right)$$

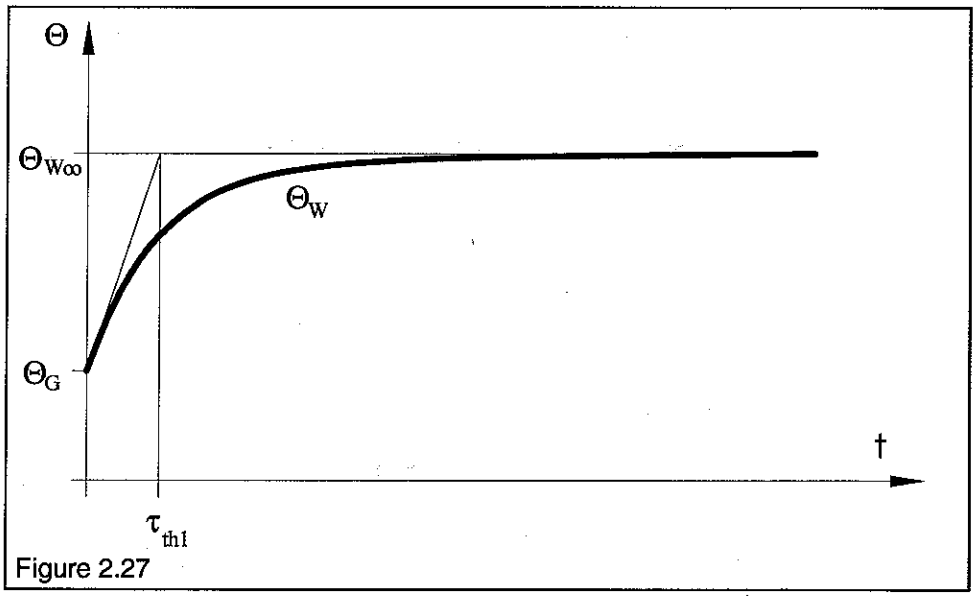

Figure 2.27

At steady state, that is $t \rightarrow \infty$, we get the winding temperature $\Theta_W$

Eq. 2.99 $$\Theta_{W\infty} = \Theta_G + P_V R_{th1}$$

For the temperature rise of the housing the same considerations apply, therefore, analogous to Eq 1.120 we define a thermal time constant $\tau_{th2}$

Eq. 2.100 $$\tau_{th2} = R_{th2} C_G = R_{th2} m_G c_G$$

Generally $R_{th2} > R_{th1}$, is true for the EC-motor as well, but can be improved with appropriate measures (forced cooling or increasing the cooling surface area with a heat sink).

For the housing temperature we get the relationship, analogous to Eq. 1.121

Eq. 2.101 $$\Theta_G = \Theta_U + P_V R_{th2}\left(1 - e^{-\frac{t}{\tau_{th2}}}\right)$$

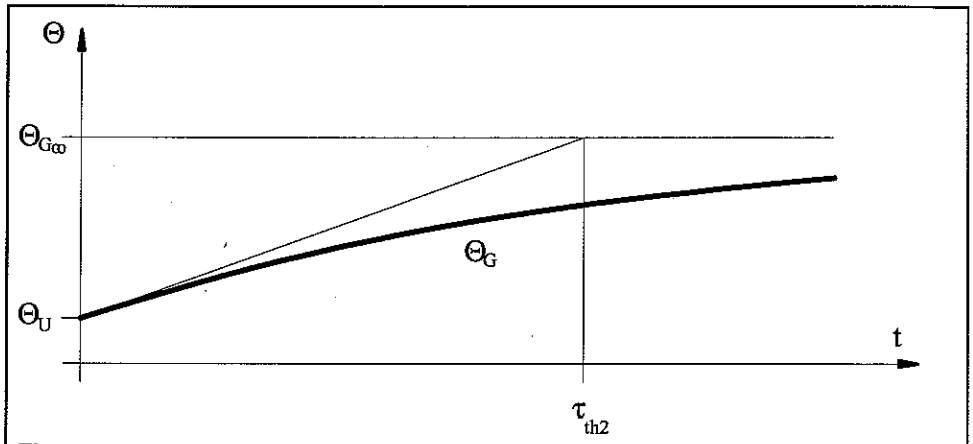

Figure 2.28

For steady state, that is $t \to \infty$, we get the housing temperature $\Theta_G$

Eq. 2.102 $$\Theta_{G\infty} = \Theta_U + P_V R_{th2}$$

### 2.5.7.4. Cooling

As in section 1.7.7.4, for a cooling process starting point we will assume that the winding is at its maximum permissible temperature and there are no further power losses generated. Therefore we get the following relationship for winding cooling

Eq. 2.103 $$\Theta_W = \Theta_G\left(1 - e^{-\frac{t}{\tau_{th1}}}\right) + \Theta_{W\,max} e^{-\frac{t}{\tau_{th1}}}$$

At steady state near the end of the cooling cycle, as $t \to \infty$, we get the winding temperature as

Eq. 2.104 $$\Theta_{W\infty} = \Theta_G$$

### 2.5.7.5. Intermittent Use

The derivation in section 1.7.7.5 and its results are fully applicable to the EC-motor. For periodic intermittent use we get an average winding temperature proportional to the square of effective current.

$$\Theta_m \approx \frac{1}{T}\int_0^T i^2 dt = I_{eff}^2$$

# Appendix

## A1. SI Units and Derived Units

Mass .....[kg]
Length.....[m]
Voltage .....[V]
Current.....[A]
Temperature .[K]
Angle .....[rad]
Time.....[s]

[H .....=Vs/A]
[J.....=Ws .....=$kgm^2/s^2$]
[$J/m^3$.....=$N/m^2$..... =$kg/ms^2$]
[N .....=$kgm/s^2$]
[Nm .....=$kgm^2/s^2$]
[T .....= $Vs/m^2$]
[W .....=Nm/s..... =$kgm^2/s^3$]
[Ws .....=Nm .....=$kgm^2/s^2$]
[Wb .....=Vs]
[Ω..... =V/A]

## A2. Vector Quantities

dA .....[$m^2$] ..... Surface Element Vector
B .....[T] ..... Induction Vector
F .....[N]..... Force Vector
$F_x$.....[N]..... x component of the Force Vector
$F_y$.....[N]..... y component of the Force Vector
H.....[A/m]..... Field Strength Vector
I.....[A]..... Current Vector
$\ell$.....[m] ..... Conductor Length Vector
M.....[Nm]..... Torque Vector
$M_z$ .....[Nm]..... z component of the Torque Vector
r .....[m] ..... Position Vector
$r_x$.....[m] ..... x component of the Position Vector
$r_y$.....[m] ..... y component of the Position Vector
v.....[m/s]..... Speed Vector

## A3. Scalar Quantities

A .....[$m^2$] ..... Surface
$A_L$ .....[$m^2$] ..... Air Gap Surface
$A_M$ .....[$m^2$] ..... Magnet Surface
$A_{Ra}$.....[$m^2$] ..... Magnetic Return Path Surface
a.....[m] ..... Length
α .....[$W/m^2K$]..... Coefficient of Heat Transmission
$\alpha_{Cu}$.....[$K^{-1}$]..... Temperature Resistance Coefficient for Copper (0.00392 $K^{-1}$)
$B_A$ .....[T] ..... Magnet Material Induction at Operating Point A
$B_L$ .....[T] ..... Air Gap Induction
$B_M$ .....[T] ..... Magnet Material Induction
$B_r$.....[T]..... Residual Induction
$B_{Ra}$.....[T] ..... Outer Magnetic Return Path Induction
$B_W$.....[T] ..... Eddy Current Induction
$(BH)_{max}$ ...[$J/m^3$]..... Magnetic Energy Density, max. Energy Product
$B_o$ .....[T] ..... Air gap Induction Amplitude
b.....[m] ..... Length
β..... [rad]..... Angle

$C_G$ .....[Ws/K]..... Heat Capacity of the Stator Housing
$C_R$ .....[Ws/K]..... Heat Capacity of the Rotor Winding
$C_S$.....[Ws/K]..... Heat Capacity of the Stator
$C_s$ .....[W/m$^2$K$^4$] ... Coefficient of Radiant Heat Transfer
$C_W$.....[Ws/K]..... Heat Capacity of the Winding
$c_H$ ..... ..... Hysteresis Material Constant
$c_G$ .....[Ws/kgK]..... Specific Heat of the Stator Housing (Fe = 460Ws/kgK)
$c_R$ .....[Ws/kgK]..... Specific Heat of the Rotor Winding (Cu = 385Ws/kgK)
$c_S$ .....[Ws/kgK]..... Specific Heat of the Stator (Fe = 460Ws/kgK)
$c_T$.....[Nm/rad] ..... Torsion Spring Constant
$c_W$ .....[Ws/kgK]..... Specific Heat of the Stator Winding(Cu = 385Ws/kgK)
$c_a$..... ..... Cooling Constant of Integration
$c_e$..... ..... Warming Constant of Integration
$c_1$..... ..... Axial Induction Reduction Correction Factor
c5.....[Nms]..... Damping Moment
$\gamma$.....[kg/m$^3$] ..... Density

D.....[m] ..... Sheet Metal Thickness
d.....[m] ..... Material Thickness
$\eta$ ..... ..... Efficiency
$\eta_{max}$..... ..... Maximum Efficiency

E .....[V]..... emf Induced in the Rotor
$E_W$.....[V/m]..... Electronic Field Strength
$E_{ph}$ .....[V]..... Instantaneous Value of emf Induced in a Phase
dE .....[V]..... Induced Voltage
$e_i$.....[V]..... General emf Induced in a Conductor
$e_{iD}$ .....[V]..... Voltage Induced in a Straight Conductor
$e_{iR}$ .....[V]..... Voltage Induced in a Rhomb

F .....[N]..... Force
dF .....[N]..... Force
$f(\varphi_o)$..... ..... Auxiliary Function

$\Phi$.....[Wb]..... Magnetic Flux
$\Phi_I$.....[Wb]..... Magnetic Flux Through Rhomb Half I
$\Phi_{II}$ .....[Wb]..... Magnetic Flux Through Rhomb Half II

$g(\varphi_o)$..... ..... Auxiliary Function

$H_A$.....[A/m]..... Magnet Field Strength at Operating Point A
$H_K$.....[A/m]..... Anisotropic Field Strength
$H_L$ .....[A/m]..... Field Strength in the Air Gap
$H_M$ .....[A/m]..... Field Strength in the Magnet
$H_W$.....[A/m]..... Eddy Current Field Strength
$H_{Wo}$.....[A/m]..... Eddy Current Field Strength Upper Sheet Metal Half
$H_{Wu}$.....[A/m]..... Eddy Current Field Strength Lower Sheet Metal Half
$_BH_C$.....[A/m]..... Coercive Field Strength

I.....[A]..... Current
$I_{eff}$.....[A]..... Effective Current Value
$I_H$.....[A]..... Stall Current
$I_{u,v,w}$ .....[A]..... Phase Current
$I_W$ .....[A]..... Eddy Current
$I_o$.....[A]..... No Load Current
i.....[A]..... Instantaneous Current

$J_b$ .....[$kgm^2$]..... Load Moment of Inertia
$J_R$ .....[$kgm^2$]..... Rotor Moment of Inertia

$\varphi$ .....[rad] ..... Angle
$\varphi_o$ .....[rad] ..... Starting Angle
$d\varphi$ .....[rad] ..... Differential Angle Element

k..... ..... Number of Collector Segments
$k_M$.....[Nm/A] ..... Torque Constant
$\kappa$.....[$\Omega$/m]..... Electric Conductivity

$L_T$ .....[H]..... Winding Segment Induction
$\ell$.....[m] ..... Conductor Length
$\ell_D$ .....[m] ..... Straight Conductor Length
$\ell_L$ .....[m] ..... Air gap Length
$\ell_M$ .....[m] ..... Magnet Length
$\lambda$..... [W/mK]..... Coefficient of Thermal Conductivity

M.....[Nm]..... Torque
$M_B$ .....[Nm]..... Acceleration Torque
$M_b$.....[Nm]..... Load Torque
$M_\eta$ .....[Nm]..... Torque at Maximum Efficiency
$M_{iH}$ .....[Nm]..... Ideal Stall Torque
$M_{iHmin}$ .....[Nm]..... Minimum Stall Torque
$M_P$ .....[Nm]..... Torque at Maximum Power
$M_V$ .....[Nm]..... Loss Torque
MVA.....[Nm]..... Stand Still Loss Torque Approximation
$M_{Vo}$ .....[Nm]..... No Load Loss Torque
$M_{Vk}$ .....[Nm]..... Collector Friction Torque
$M_T$ .....[Nm]..... Return Torsion Torque
$m_R$ .....[kg] ..... Mass of the Rotor (Winding)
$m_S$ .....[kg] ..... Mass of the Stator
$m_W$ .....[kg] ..... Mass of the Stator Winding
$\mu_o$.....[Vs/Am]..... Magnetic Field Constant (1.256E-6 Vs/Am)
$\mu_r$ ..... ..... Relative Permeability
$\mu_{ra}$ ..... ..... Relative Starting Permeability

$n_b$.....[$s^{-1}$] ..... Load Rotational Speed
$n_i$.....[$s^{-1}$] ..... Ideal No Load Rotational Speed
$n_o$.....[$s^{-1}$] ..... No Load Rotational Speed
$\nu$..... [$m^{-1}$]..... Winding Density
$\Delta n/\Delta M$ .....[$s^{-1}$/Nm]..... Speed/Torque Gradient

P .....[W]..... Output Power
$P_{Fe}$.....[W]..... Iron Losses
$P_{FeH}$ .....[W]..... Iron Hysteresis Losses
$P_{FeW}$.....[W]..... Iron Eddy Current
$P_J$ .....[W]..... Joule's Power Loss
$P_{max}$ .....[W]..... Maximum Output Power
$P_{mech}$ .....[W]..... Mechanical Power
$P_R$.....[W]..... Friction Power
$P_V$.....[W]..... Power Dissipation
$P_{Vzul}$ .....[W]..... Maximum Allowable Power Dissipation
$P_W$.....[W]..... Rotating Field Power
$P_{WV}$ .....[$W/m^3$]..... Rotating Field Power Density
$P_{zu}$ .....[W]..... Input Power

$Q_W$ ..... [As] ..... Electric Charge
$\Theta$ ..... [K] ..... Temperature
$\Theta_G$ ..... [K] ..... Housing Temperature
$\Theta_{G\infty}$ ..... [K] ..... Housing Temperature as Time Approaches Infinity
$\Theta_K$ ..... [K] ..... Body Temperature
$\Theta_m$ ..... [K] ..... Average Temperature
$\Theta_{max}$ ..... [K] ..... Maximum Temperature
$\Theta_{min}$ ..... [K] ..... Minimum Temperature
$\Theta_R$ ..... [K] ..... Rotor Temperature
$\Theta_{R\infty}$ ..... [K] ..... Rotor Temperature as Time Approaches Infinity
$\Theta_{Rmax}$ ..... [K] ..... Maximum Rotor Temperature
$\Theta_{S\infty}$ ..... [K] ..... Stator Temperature as Time Approaches Infinity
$\Theta_S$ ..... [K] ..... Stator Temperature
$\Theta_U$ ..... [K] ..... Ambient Temperature
$\Theta_W$ ..... [K] ..... Winding Temperature
$\Theta_{W\infty}$ ..... [K] ..... Winding Temperature as Time Approaches Infinity
$\Theta_{Wmax}$ ..... [K] ..... Maximum Winding Temperature
$\Delta\Theta$ ..... [K] ..... Temperature Differential

$R_{ph}$ ..... [$\Omega$] ..... Phase Resistance
$R_{ph\Theta}$ ..... [$\Omega$] ..... Phase Resistance at Temperature $\Theta$
$R_{ph\Theta max}$ ..... [$\Omega$] ..... Phase Resistance at Temperature $\Theta_{max}$
$R_{Rot}$ ..... [$\Omega$] ..... Rotor Resistance
$R_{th}$ ..... [K/W] ..... Thermal Resistance
$R_{th1}$ ..... [K/W] ..... Thermal Resistance Rotor-Stator
$R_{th2}$ ..... [K/W] ..... Thermal Resistance Stator-Surroundings
$R_\Theta$ ..... [$\Omega$] ..... Rotor Resistance at Temperature $\Theta$
$R_{\Theta max}$ ..... [$\Omega$] ..... Rotor Resistance at Maximum Rotor Temperature
$R_{w\Theta}$ ..... [$\Omega$] ..... Winding Resistance at Temperature $\Theta$
$R_{25}$ ..... [$\Omega$] ..... Rotor Resistance at 25°C
$\rho$ ..... [m/$\Omega$] ..... Resistivity

$S_W$ ..... [A/m$^2$] ..... Current Density of the Eddy Currents
ds ..... [m] ..... Rotor Circumferential Length Element
$\sigma$ ..... ..... Magnetic Leakage Factor

T ..... [s] ..... Time Constant
$T_R$ ..... [s] ..... Vibration Period of the EC-Rotor
t ..... [s] ..... Time
$\tau$ ..... ..... Magnetic Potential Drop Factor
$\tau_m$ ..... [s] ..... Mechanical Time Constant of the Rotor
$\tau_{mges}$ ..... [s] ..... Mechanical Time Constant of the Whole System
$\tau_{th1}$ ..... [s] ..... Thermal Time Constant of the Rotor
$\tau_{th2}$ ..... [s] ..... Thermal Time Constant of the Stator

U ..... [V] ..... Motor Voltage
$u_i$ ..... [V] ..... Motion Inducted Voltage in a Winding Segment
$u_L$ ..... [V] ..... Self Inducted Voltage in a Winding Segment

$V_L$ ..... [m$^3$] ..... Air Gap Volume
$V_M$ ..... [m$^3$] ..... Magnet Volume
$v_k$ ..... [m/s] ..... Collector Circumferential Speed
dV ..... [m$^3$] ..... Volume Element

$W_L$ ..... [Ws] ..... Air Gap Energy
$W_{LT}$ ..... [Ws] ..... Energy Stored in a Winding Segment

| | | |
|---|---|---|
| $W_M$ | [Ws] | Magnet Energy |
| $W_{mech}$ | [Ws] | Mechanical Work |
| $W_W$ | [Ws] | Energy of the Rotating Field |
| w | | Winding Number |
| $w_T$ | | Winding Number of a Winding Segment |
| $\omega$ | [rad/s] | Angular Velocity |
| $\psi$ | [rad] | Magnetic Torsion Angle |